Research Square

Preprints are preliminary reports that have not undergone peer review.
They should not be considered conclusive, used to inform clinical practice,
or referenced by the media as validated information.

Quantifying pixel- and patch-scale *Spartina patens* dynamics during salt marsh restoration using multispectral UAV imagery

Gregory S. Norris

gnorris1@unb.ca

University of New Brunswick https://orcid.org/0000-0003-0282-1999

Myriam A. Barbeau

University of New Brunswick

Armand LaRocque

University of New Brunswick

Brigitte Leblon

Lakehead University

Alan R. Hanson

Canadian Wildlife Service

Research Article

Keywords: High-marsh development, plant patch dynamics, coastal wetlands, drone imagery, pixel-based Random Forest image classification, post-classification change detection.

Posted Date: November 23rd, 2026

DOI: https://doi.org/10.21203/rs.3.rs-11763202/v1

License: This work is licensed under a Creative Commons Attribution 4.0 International License.
Read Full License

Additional Declarations: The authors declare no competing interests.

Abstract

As a salt marsh restoration progresses, the temporal transition from low marsh to high-marsh vegetation is an ecologically important stage reflecting increased elevation and reduced tidal inundation, as well as associated changes in ecosystem functioning and services including faunal community composition, fish accessibility, coastal protection, and carbon burial. However, quantifying this transitional process is challenging because vegetation change often occurs at fine spatial scales. We used high-resolution, multispectral uncrewed aerial vehicle (UAV) imagery and pixel-based random forest classification to generate annual land cover maps at two managed realignment salt marsh restoration sites in the Bay of Fundy, Atlantic Canada, over three growing seasons (2020–2022). High classification accuracy (overall accuracy 90.1–95.2%) enabled detailed assessment of vegetation change, showing expansion of the foundational high-marsh zone grass *Spartina patens*. Patch-based analyses showed that persistent *S. patens* patches formed stable patch cores that gradually increased in area through time, while gains and losses were concentrated along patch edges. Most gains occurred in areas previously occupied by the low marsh cordgrass *S. alterniflora*, whereas direct colonization of mud was uncommon. Ancillary image-derived predictor analysis focused on the congeneric *Spartina* grasses showed that the most important spectral wavelength bands, vegetation indices, and textural features differed between *S. patens* comparisons with sparse and dense *S. alterniflora*. Together, our findings demonstrate that combining pixel-based UAV classifications, patch-based analyses, and evaluation of image-derived predictors improves understanding of vegetation succession and provides a transferable framework for monitoring high-marsh development in restoring salt marshes.

Introduction

Salt marshes are characterized by distinct low- and high-marsh vegetation communities that reflect biogeochemical processes and affect ecosystem functioning and services. Salt marsh plant distributions are influenced by elevation, hydroperiod, edaphic conditions, species interactions such as competitive displacement, and disturbance, resulting in vegetation zonation, plant patch expansion and contraction, and edge-mediated transitions (Bertness, 1991; Bertness & Ellison, 1987; Pennings & Callaway, 1992). Vegetation-geomorphology feedbacks are fundamental to marsh persistence, as plant growth enhances sediment trapping and surface elevation, while elevation gradients structure plant community composition and productivity (Cahoon et al., 2021; Gedan et al., 2011; Kirwan & Megonigal, 2013; Morris et al., 2002). Furthermore, vegetation zones contribute differently to salt marsh ecosystem services, including coastal protection, carbon sequestration, nutrient cycling, and habitat for diverse wildlife communities (Barbier et al., 2011; Gallant et al., 2020; Garzon et al., 2019). For example, the low marsh provides regularly accessible habitat for fish and mobile crustaceans and shows greater export of organic detritus because of its frequent tidal inundation, whereas the high marsh generally contributes more to denitrification, sediment retention, shoreline stability, and elevation capital through denser vegetation and less frequent inundation (Baker et al., 2020; Bouchard & Lefeuvre, 2000; Cahoon et al., 2019; Ooi et al., 2022; Rozas, 1995; Ziegler et al., 2021). Additionally, the relative extent and distribution of vegetation zones influence marsh persistence and resilience to sea-level rise, coastal squeeze, and

other stresses (Colombano et al., 2021; Wasson et al., 2019). Finally, salt marsh restoration projects are increasingly being implemented worldwide, and the desired balance between low- and high-marsh habitat depends on restoration objectives and the ecosystem services being prioritized (Adams et al., 2021; De Lauretis et al., 2026; Waltham et al., 2021). Thus, quantifying how vegetation assemblages establish, spread, and transition from low to high marsh following tidal reconnection is essential for evaluating restoration trajectories, ecosystem functioning and service provisioning, and resilience to environmental stressors.

In Maritime Canada, extensive diking and drainage for agriculture have resulted in widespread salt marsh loss. The Bay of Fundy is characterized by some of the world's largest tidal ranges, which shape regional coastal geomorphology and create unique conditions for restoration trajectories and monitoring (Bowron et al., 2012; Desplanque & Mossman, 2004; van Proosdij et al., 2023). A focus of restoration work in this region has been in Aulac, New Brunswick, where tidal reconnection of two formerly diked pastureland sites occurred in 2010 through managed realignment (Boone et al., 2017; Millard et al., 2013). Long-term monitoring following dike breaching documented rapid vegetation change across the restoring marsh platform (Norris et al., 2022b; Virgin et al., 2020). Prior to breaching, patches of freshwater cordgrass *Spartina pectinata* (syn. *Sporobolus michauxianus*) were present within the diked agricultural land and briefly persisted following tidal inundation. Beginning in 2012, saltwater cordgrass *Spartina alterniflora* (syn. *Sporobolus alterniflorus*, Bortolus et al., 2019; Peterson et al., 2014) colonized the site through mainly rhizome expansion from mature plants that likely colonized via ice rafting rather than seedling establishment, forming discrete patches. These patches spread, and along with en masse natural seeding events in 2014–2015, coalesced into a largely continuous low-marsh zone. By 2017, salt marsh hay *Spartina patens* (syn. *Sporobolus pumilus*) began establishing as scattered interior patches as surface elevation increased, while also expanding from higher-elevation dike margins into the marsh interior. This progression is consistent with salt marsh restoration models in which low-marsh vegetation establishes rapidly following tidal reconnection, and high-marsh communities develop more gradually through competitive interactions as sediment accumulation creates suitable conditions (Bertness, 1991; Mossman et al., 2012; Roman & Burdick, 2012). Because *S. patens* is strongly associated with high-marsh environments in the region, its spread and persistence are indicators of high-marsh development during restoration. Understanding how high-marsh species expand within low-marsh areas would provide insight into marsh succession and long-term restoration trajectories.

Monitoring vegetation dynamics across restored marsh platforms is challenging due to logistical constraints and variable access conditions, which can limit the spatial coverage and repeatability of field surveys (Shawler et al., 2025). Satellite remote sensing provides broad coverage but often lacks the spatial resolution needed to resolve the fine-scale patch expansion, boundary shifts, and internal heterogeneity typical of marsh vegetation (Adam et al., 2010; Klemas, 2013). Uncrewed aerial vehicles (UAVs) equipped with multispectral sensors provide an intermediate approach by combining complete site coverage with centimeter-scale spatial resolution and spectral information that supports vegetation classification (Alvarez-Vanhard et al., 2021; Guo et al., 2016). UAV imagery has been applied in coastal wetlands to map vegetation communities and species distributions, evaluate classification approaches

using spectral bands and vegetation indices, and improve discrimination among marsh plants across elevation gradients (Huang et al., 2023; Kim et al., 2023a; Norris et al., 2024; Routhier et al., 2023). UAV data have also been used to estimate aboveground biomass, generate high-resolution elevation models, and characterize marsh structure and ecosystem properties (Curcio et al., 2024; Doughty & Cavanaugh, 2019; Pinton et al., 2021; Taddia et al., 2021). These practices can support monitoring of marsh restoration and ecosystem change through time when UAV surveys are repeated (Dronova et al., 2021; Haskins et al., 2021; Thomsen et al., 2021). In some cases, repeated UAV surveys have enabled multi-temporal mapping of vegetation development and species distributions in restored marsh systems (Nardin et al., 2021; Windle et al., 2023) and have been used to quantify patch-scale expansion of *S. alterniflora* (Zhu et al., 2019).

Despite these advances, relatively few studies have used repeated species-level UAV classifications to investigate the ecological processes underlying vegetation change in restored salt marshes. Existing studies have largely focused on vegetation mapping, biomass estimation, ecosystem properties, or documenting broad changes in species distributions (Doughty & Cavanaugh, 2019; Li et al., 2021; Nardin et al., 2021; Windle et al., 2023). However, less attention has been given to quantifying species transitions, patch persistence, expansion, contraction, and vegetation replacement through time. Consequently, the localized processes that drive transitions from low- to high-marsh vegetation during marsh succession remain poorly understood. Quantifying these processes also depends on accurately distinguishing spectrally similar vegetation communities. Previous studies have shown that red-edge wavelengths are particularly sensitive to vegetation condition and inundation in marsh environments (Turpie, 2013), while multispectral imagery, vegetation indices, and textural features have all been shown to improve wetland vegetation classification and biomass estimation (Adam et al., 2010; Kim et al., 2023a; Li et al., 2021; Norris et al., 2024). Less is known about which spectral regions and predictor types are most effective for discriminating closely related salt marsh species such as *S. patens* and *S. alterniflora*. Understanding these relationships would not only improve classification accuracy but also guide sensor selection and the design of future UAV monitoring programs.

Our study addressed the above gaps by integrating multi-temporal multispectral UAV imagery with species-level classification, patch-based ecological analysis, and image-derived predictor analysis to investigate the transition from low- to high-marsh vegetation during a salt marsh restoration at Aulac. This approach enabled high-marsh development to be examined across multiple spatial scales, from whole-site changes in vegetation composition and species transitions to localized patterns of *S. patens* persistence, expansion, contraction, and replacement along patch edges. We evaluated the relative importance of image-derived predictors for distinguishing between land covers dominated by the congeneric grasses *S. patens* and *S. alterniflora*, which linked ecological interpretation with the image-derived information required for reliable species discrimination. Thus, our objectives were to: (1) generate annual land cover classifications for two restoring salt marsh sites using a random forest (RF) classifier applied to multi-temporal (June–August) predictors derived from multispectral imagery; (2) quantify site-wide vegetation composition and pixel-level land cover class transitions between 2020–2021 and 2021–2022; (3) quantify *S. patens* persistence, gains, losses, and patch-scale expansion using

trajectory analyses of selected *S. patens* patches and vegetation dynamics along patch edges; and (4) evaluate discrimination between *S. patens* and *S. alterniflora* land covers by identifying which spectral bands, vegetation indices, and textural features most effectively distinguished the two congeneric *Spartina* grasses. By resolving vegetation dynamics at both pixel and patch scales, our approach supports high-resolution monitoring of restoration trajectories and provides a framework for quantifying fine-scale vegetation change often missed by conventional sampling or satellite imagery. Such detailed analyses provide the ecological context needed to subsequently quantify how shifts in plant communities influence ecosystem function and services as restored salt marshes mature.

Methods

Study sites

The study area is in Aulac, New Brunswick, Canada, at the head of the Cumberland Basin within the Bay of Fundy (Fig. 1). The region experiences semi-diurnal, megatidal amplitudes ranging from ~ 9–13 m (Fisheries and Oceans Canada, 2026). The salt marsh restoration project includes two sites (Restoration East and Restoration West), which are ~ 5.5 and ~ 11.0 ha in size, respectively. By the beginning of our study period, the sites were largely dominated by *Spartina alterniflora*, while *S. patens* occurred in patches within the marsh interior as well as along higher-elevation dike edges (Norris et al., 2022b; Norris et al., 2024; Virgin et al., 2020). The dike areas also supported other higher elevation species, including *S. pectinata*.

Data collection and imagery acquisition

Field data collection

We collected field data to support training and validation of land cover classifications. Stratified random sampling was conducted at both sites using 0.5 m × 0.5 m (0.25 m²) quadrats positioned along 3–4 transects per site during June, July, and August field campaigns in 2020–2022 (Norris et al., 2024; Virgin et al., 2020). Additional quadrats were placed to ensure representation of all observable land cover types (Table 1). Sampling was timed to capture key phenological stages from early vegetation emergence (June) through peak growth and flowering (July–August), but prior to senescence (September; Norris et al., 2022b). At each sampling location, we recorded GPS coordinates using a handheld unit with approximately 3 m positional accuracy, documented land cover classes, identified and counted plant stems, and took ground photographs.

Multispectral UAV imagery acquisition

We acquired multispectral imagery using a MicaSense dual-camera system mounted to a DJI Matrice 200 V2 UAV (described in Norris et al., 2022a; Norris et al., 2024) (Fig. 2). The sensor captured imagery across ten spectral bands spanning blue, green, red, red-edge, and near-infrared wavelengths. Flights

were conducted at an altitude of 100 m with approximately 80% front and side overlap, resulting in orthomosaics with a spatial resolution of ~ 7.4 cm. We scheduled image acquisition to align with field sampling campaigns, minimize tidal inundation and shadow effects, and obtain site coverage under as consistent illumination conditions as possible (Table S1). We photographed a calibrated reflectance panel prior to each flight for radiometric calibration (Aasen et al., 2015).

Image pre-processing and predictor variable extraction

We processed multispectral imagery in Pix4D photogrammetric software, where radiometric calibration and mosaicking were performed to generate georeferenced reflectance orthomosaics for each site and acquisition date (Fig. 2) (see Norris et al., 2024 for a detailed description of processing options). Orthomosaics were subsequently orthorectified and co-registered in PCI Catalyst using stable, non-changing landscape features (e.g., terrestrial dike edges, boulders) to ensure spatial alignment across monthly and annual image acquisitions. For each site, orthomosaics from June, July, and August were combined into multi-temporal stacks for each monitoring year (2020–2022) to incorporate seasonal phenological variation into the annual classifications. Spectral reflectance bands were used to derive vegetation indices and neighborhood-based textural metrics for each site across all monthly and annual observations prior to classification. A total of 28 vegetation indices were derived from the multispectral imagery (Norris et al., 2024; Table S2), with several calculated using multiple spectral band combinations (e.g., different red-edge and visible bands), resulting in two or three index variants per formula. These indices capture variation in vegetation cover and greenness by exploiting spectral contrasts between vegetation and background reflectance (Richardson & Wiegand, 1977; Rouse et al., 1974). Textural features were calculated using a gray-level co-occurrence matrix (GLCM) approach (Haralick et al., 1973) to quantify local spatial variation in reflectance. For each of the 10 spectral bands, 10 GLCM-derived metrics (e.g., contrast, homogeneity, entropy) were computed using a 9 × 9-pixel kernel, resulting in 100 textural features per image (Table S2). These features have been shown to improve discrimination among vegetation, wrack, and bare muddy substratum (Norris et al., 2022a). In total, 138 predictor layers were produced per monthly image (10 reflectance bands, 28 vegetation indices, and 100 textural features), and 414 predictor layers per site-year combination following multi-temporal stacking.

Classification framework

Training and validation data

We defined and used seven land cover classes across sites (Restoration East, Restoration West) and years (2020–2022; Table 1). Vegetation classes included *S. patens*, dense *S. alterniflora*, sparse *S. alterniflora*-mixed low-stature vegetation, and *S. pectinata*-elevated dike edge vegetation. The sparse *S. alterniflora*-mixed class was dominated by low density *S. alterniflora*, with occasional contributions from other low-stature marsh species. The *S. pectinata*-elevated dike edge class represented *S. pectinata* stands along the marsh-terrestrial transition and included adjacent terrestrial vegetation where present.

Surface-cover classes included mud, rock, and wrack, with the wrack class representing accumulated tidal organic deposits such as dead vegetation mats and woody debris (Table 1; Fig. 3).

We delineated training and validation samples as polygons across each site's orthomosaics, guided by field observations (GPS coordinates and ground photographs) (Fig. 2). These polygons represented relatively homogeneous patches of each land cover class and were typically digitized as approximately 5 × 5-pixel squares (~ 0.14 m²), although smaller or irregularly shaped polygons were used where boundaries between classes were more complex. Training and validation polygons were delineated independently for each year to reflect year-specific imagery, resulting in areas that were often comparable but not identical across years. Training and validation datasets were generated by randomly assigning 60% of polygons to training and 40% to validation for each year independently, while maintaining spatial separation to reduce spatial dependence and potential overestimation of accuracy (Roberts et al., 2017). Polygons were subsequently converted to pixel-level samples for both training and validation datasets by extracting all pixels contained within their boundaries. Sample sizes varied among classes and years in accordance with class extent while ensuring that all classes were represented (Fig. 4).

Classification

We generated pixel-based land cover classifications using a RF supervised classification approach conducted in R using the *randomForest* package (Liaw & Wiener, 2002; R Core Team, 2025). RF was used because it can handle correlated predictors and complex, nonlinear class separations (Belgiu & Drăguţ, 2016; Breiman, 2001; Maxwell et al., 2018). A pixel-based approach was selected because the analysis focused on pixel-level transitions, persistence of *S. patens* patch cores, and vegetation dynamics along patch edges across repeated UAV surveys. Although pixel-based approaches can be susceptible to speckle, a "salt-and-pepper" pattern caused by isolated misclassified pixels that can artificially fragment vegetation patches, they are well suited for quantifying fine-scale spatial change and patch dynamics (Blaschke, 2010; Maxwell et al., 2018). Previous coastal wetland studies have shown that pixel-based classifications can match or outperform object-based approaches for heterogeneous vegetation (Martínez Prentice et al., 2021; Norris et al., 2024). Separate RF models were developed for each combination of site and year (2020–2022) using the multi-temporal predictor stacks (Table S2). RF models were constructed using 500 decision trees with the default mtry parameter (the number of predictor variables randomly considered at each split within each tree) set as the square root of the total number of predictors. Bootstrap aggregation produced out-of-bag (OOB) samples that provided internal estimates of classification performance and enabled assessment of predictor importance using mean decrease in accuracy. For each site-year model, predictors were ranked by mean decrease in accuracy, and the 10 highest-ranked predictors were summarized by predictor type (reflectance, vegetation index, or texture) and acquisition month. Following model training, RF predictions were applied to the full images to generate classified maps for each site and year combination.

Accuracy assessment

We evaluated classification accuracy using both internal and independent validation approaches (Fig. 2). Internal model performance was assessed using OOB estimates generated during model construction, from which confusion matrices and associated accuracy metrics were derived. Independent accuracy assessments were conducted using the spatially independent validation data. Reference labels from validation data were compared with classified map predictions to generate confusion matrices for each site and year combination. From both OOB and independent confusion matrices, overall accuracy (the proportion of all samples correctly classified), average accuracy (the mean accuracy across all land cover classes), class-specific user's accuracy (related to errors of commission) and producer's accuracy (related to errors of omission), and the kappa coefficient (a measure of agreement between classified and reference data after accounting for chance agreement) were calculated following standard accuracy assessment procedures (Congalton & Green, 2009). OOB results indicated high internal classification performance (> 99% overall accuracy; Tables S3–S8); independent validation accuracy is used as the main measure of classification performance in the results section.

Post-classification ecological analyses

Vegetation composition

We conducted post-classification ecological analyses using the annual land cover maps to quantify vegetation composition and transition dynamics (Fig. 2). Analyses were performed at the native pixel resolution (~ 7.4 cm) to retain fine-scale spatial structure relevant to salt marsh vegetation processes including zonation. Annual class composition was calculated as the proportion of pixels assigned to each land cover class within each combination of site and year (2020–2022), enabling comparison of vegetation composition through time. Temporal change dynamics were evaluated using pixel-level cross-tabulation of classified rasters between monitoring intervals (2020–2021 and 2021–2022; Olofsson et al., 2014). Transition matrices quantified class persistence and change among classes. Although pixel-level analyses captured site-wide vegetation dynamics, fine-resolution classifications can be affected by speckle and classification noise (Maxwell et al., 2018). We therefore also conducted analyses of vegetation patch dynamics.

Plant patch dynamics

We examined spatial dynamics of *S. patens* to evaluate persistence, gains, losses, and localized patch expansion using two complementary approaches. Stability maps were generated by overlaying classified maps and identifying pixels that retained a *S. patens* classification across a monitoring interval. These maps were used to identify persistent patches and provide a consistent basis for evaluating patch dynamics through time. (i) Patch trajectory analysis focused on a subset of *S. patens* patches identified within the restoration sites in the field (Norris et al., 2022b; Stack Mills et al., 2023). These patches were selected based on GPS-located field observations and confirmed using stability maps to persist

throughout the monitoring period (2020–2022). We identified one and eleven persistent *S. patens* patches within Restoration East and Restoration West, respectively, corresponding to patches previously identified and monitored in the field. For these patches, polygons were delineated annually and patch area was calculated for each year. This approach prioritized consistency with field observations over map-wide filtering and allowed direct tracking of individual patch dynamics through time. (ii) For interval-based analyses (2020–2021 and 2021–2022), persistent pixels identified from stability maps were converted to vector polygons and dissolved into contiguous areas of stable *S. patens*. Following removal of polygons smaller than 0.25 m² (the size of the field quadrat), the resulting features were defined as patch cores. Patch edges were operationally defined as a 2-m buffer surrounding each patch core, where expansion, contraction, and vegetation replacement (including competitive replacement) were likely to occur (Angelini et al., 2011; Bertness, 1991; Norris et al., 2022b). Pixel-level transitions among non-*S. patens* classes within patch-edge buffers were quantified to identify vegetation classes contributing to observed gains and losses of *S. patens*.

Pairwise analysis of *Spartina* predictor variables

We conducted comparisons between *S. patens* and *S. alterniflora* (both dense and sparse classes) to identify the predictor variables that most effectively distinguished these ecologically consequential, congeneric salt marsh vegetation classes. Training and validation polygons were rasterized, individual pixels were converted to point features, and predictor values were extracted from the annual multispectral predictor stacks. Because neighbouring pixels originating from the same polygon were not statistically independent, one pixel was randomly selected from each polygon to reduce spatial dependence among samples (Roberts et al., 2017). Comparisons were performed separately for each restoration site and year combination, with *S. patens* evaluated independently against each of the dense and sparse *S. alterniflora* classes. To minimize potential bias associated with unequal sample sizes, the larger vegetation class in each comparison was randomly subsampled to match the smaller class, resulting in 81–165 observations per class across site-year combinations.

Differences in predictor values between congeneric *Spartina* classes were examined using Welch's two-sample *t* statistic (Welch, 1947), which accounts for unequal variances between groups. For each predictor variable, we used the absolute value of Welch's *t* statistic to rank its discriminatory ability, with larger absolute values indicating greater separation between congeneric *Spartina* classes. Predictor rankings were generated independently for each site-year combination. To facilitate interpretation, the 20 highest-ranked predictors from each site-year comparison were summarized by predictor category (reflectance, vegetation index, or textural feature) and by the spectral bands contributing to each predictor, allowing the relative importance of the original blue, green, red, red-edge, and near-infrared wavelengths to be assessed. Raw reflectance and textural predictors were assigned to their original spectral band, while vegetation indices were assigned to each spectral band used in their calculation. Band-contribution frequencies were calculated separately for each site-year comparison and summarized as the mean ± SD across the six site-year combinations for each *Spartina* comparison.

Results

Classification performance and predictor importance

Validation assessments indicated high classification accuracy (Tables 2–3). At Restoration East, overall accuracy increased from 90.1% in 2020 to 94.5% in 2022, with kappa coefficients rising from 0.88 to 0.93 and average class accuracy from 89.1% to 93.9%. At Restoration West, overall accuracy ranged from 93.6% to 95.2%, with kappa coefficients between 0.91 and 0.94 and average class accuracy between 92.4% and 94.0%. Class-specific accuracies were consistently high for dense *Spartina alterniflora* and mud at both sites. Mud had user's accuracy ranging from 91.1% to 97.0% and producer's accuracy from 95.0% to 97.5%. Rock had similarly high user's accuracy (93.3–97.0%) but lower producer's accuracy (85.5–92.4%), indicating greater omission of rock pixels. The *S. alterniflora* sparse/mixed short-stature class also showed strong performance, with user's and producer's accuracies ≥ 87.2% across all years. Misclassification within *S. alterniflora* occurred primarily between dense and sparse/mixed structural states rather than among species. *Spartina patens* had lower and more variable accuracy than other vegetation classes. At Restoration East, *S. patens* user's accuracy ranged from 83.5% to 94.0% and producer's accuracy from 71.3% to 88.4%. At Restoration West, *S. patens* user's accuracy ranged from 83.0% to 92.8% and producer's accuracy from 89.4% to 93.7%. Confusion involving *S. patens* occurred with sparse/mixed *S. alterniflora* and *S. pectinata*-elevated dike edge. Misclassifications with dense *S. alterniflora* were limited, and confusion with mud, rock, or wrack was rare. Lower producer's accuracy for *S. patens* in 2020 at Restoration East (71.3%) reflects omission errors when patches were smaller. Accuracies for the *S. pectinata*-elevated dike edge and wrack classes varied among years but were high. For *S. pectinata*, user's accuracy ranged from 79.6% to 94.2% and producer's accuracy from 88.0% to 94.5%. Wrack had user's accuracy ranging from 85.0% to 95.5% and producer's accuracy from 92.8% to 97.5%.

Predictor-importance rankings varied among site-year models but consistently highlighted the contribution of textural information (Figures S1–S2). At Restoration East, texture features accounted for all 10 top-ranked predictors in 2020 and 2021 and eight of the top 10 in 2022 (Figure S1). Rankings at Restoration West included a broader mixture of texture features, vegetation indices, and raw reflectance bands (Figure S2). Across both sites, many highly ranked predictors incorporated red-edge or near-infrared wavelengths, and predictors derived from July and August imagery were particularly prominent.

Spatial and temporal patterns of land cover (2020–2022)

Land cover maps indicated the development of elevation-driven zonation at both sites during the monitoring period (Figs. 5–6). Low-marsh interiors were dominated by *S. alterniflora*, while *S. patens* occurred both along higher-elevation dike margins and as patchy interior vegetation. The *S. pectinata*-elevated dike edge class persisted as a narrow band along the marsh-terrestrial transition. Surface-cover classes (mud, rock, wrack) were patchy and associated with lower-elevation depressions, tidal channels, and seaward marsh margins.

Temporal changes in relative cover reflected transitions between dense and sparse/mixed *S. alterniflora* classes and gradual expansion of *S. patens* (Fig. 7; Table S15). At Restoration East, dense *S. alterniflora* increased slightly from 36% of total site area in 2020 to 37% in 2021, before declining to 30% in 2022. Sparse/mixed *S. alterniflora* decreased from 19% in 2020 to 17% in 2021 and then increased to 24% in 2022. *Spartina patens* increased gradually over the years (1.8, 2.4, and 2.8% in 2020, 2021 and 2022, respectively). Mud declined slightly from 31% to 29% over the monitoring period, while rock was stable near 8% and wrack fluctuated between 3% and 4%.

Restoration West showed larger annual shifts for some classes (Fig. 7; Table S15). Dense *S. alterniflora* increased from 32% in 2020 to 55% in 2021 before declining to 38% in 2022. In contrast, sparse/mixed *S. alterniflora* decreased from 44% in 2020 to 21% in 2021 and partially rebounded to 38% in 2022. Similarly to Restoration East, Restoration West *S. patens* gradually increased (from 0.8% in 2020 to 1.5% in 2022), while mud declined (from 17% to 16%). Rock and wrack were each minor components throughout the study period in Restoration West.

Pixel-level transition dynamics of land cover classes

Pixel-level transition matrices showed higher interannual stability at Restoration East than at Restoration West (Tables S17–S22). Overall pixel agreement between consecutive years at Restoration East was 73.4% (2020–2021) and 72.5% (2021–2022), with mean class persistence exceeding 64% in both intervals. In contrast, Restoration West had lower stability, with overall agreement of 52.4% and 59.4% and mean class persistence of 55.5% and 62.8%, respectively. Across the full 2020–2022 period, cumulative agreement was higher at Restoration East (70.7%) than at Restoration West (63.6%), although the difference was less pronounced than during individual yearly intervals.

Change was driven by exchanges among vegetation classes rather than by shifts between vegetated and unvegetated states (Tables S17–S22). Transitions between the dense and sparse/mixed *S. alterniflora* land cover classes accounted for a substantial amount of interannual change, especially at Restoration West between 2020 and 2021, where exchange between these classes represented one of the largest components of change during all monitoring intervals (Tables S20–S22). Mud was highly stable through time, with 87.1–91.2% of mud pixels remaining classified as mud between consecutive years at both sites. Most transitions from mud to vegetation were to *S. alterniflora*, while mud conversion to *S. patens* was minor (Fig. 8). In contrast, reverse transitions from vegetation back to mud were rare, accounting for less than 2% of vegetated pixels during all monitoring intervals (Tables S17–S22).

Net exchanges involving *S. patens* over the study period were positive for both sites (Figs. 9–10; Tables S17–S22). At Restoration East, net transitions from *S. alterniflora* to *S. patens* totaled ~ 550 m² in 2020–2021 with an additional 250 m² in 2021–2022. These gains represented ~ 31% and 10% of the *S. patens* area present at the start of each interval, respectively (1,797 m² in 2020 and 2,441 m² in 2021). Additional net gains from *S. pectinata*-elevated dike edge contributed approximately 150 m² during 2020–2021, equivalent to about 8% of the 2020 *S. patens* area. In contrast, net exchange between *S.*

patens and *S. pectinata* was negative during 2021–2022 (approximately − 155 m²), indicating greater conversion of *S. patens* to *S. pectinata* than the reverse.

At Restoration West, net transitions from *S. alterniflora* to *S. patens* totaled ~ 210 m² during 2020–2021 with an additional 890 m² during 2021–2022. These gains corresponded to approximately 16% and 65% of the *S. patens* area present at the start of each interval, respectively (1,280 m² in 2020 and 1,370 m² in 2021). Transitions involving *S. pectinata*-elevated dike edge were variable. Net exchange was negative during 2020–2021 (approximately − 170 m²), indicating greater conversion of *S. patens* to *S. pectinata* than the reverse, but became positive during 2021–2022 (approximately + 110 m²).

Analysis of *S. patens* patch dynamics

Overlay analysis of the classified maps indicated that *S. patens* persistence was concentrated within discrete patch cores (Figs. 11–12). Stable pixels formed interior patch areas, while gains and losses were located along patch boundaries. Trajectory analysis of selected field-identified patches demonstrated fairly consistent increases in patch area from 2020 to 2022 (Fig. 13). Mean patch area increased from 1.24 m² in 2020 to 2.29 m² in 2021 and 4.04 m² in 2022, representing more than a threefold increase over the monitoring period.

Buffer areas surrounding stable *S. patens* core patches showed substantial vegetation dynamics (Fig. 14; Figure S3). Gains by *S. patens* were primarily associated with replacement of adjacent vegetation rather than spread into bare areas. In Restoration East, *S. patens* gains were dominated by replacement of *S. alterniflora*, with sparse/mixed classes contributing the largest share in both yearly intervals (274.9 m²; 377.8 m²), followed by dense *S. alterniflora* (204.3 m²; 156.6 m²). Contributions to *S. patens* gain from *S. pectinata*-elevated dike edge were also substantial (~ 195 m² in both yearly intervals). In Restoration West, a similar pattern was observed, but contributions varied more between yearly intervals. In 2020–2021, *S. patens* gains were distributed across *S. alterniflora* classes (123.3–172.8 m²), whereas in 2021–2022, *S. patens* expansion was more strongly associated with *S. pectinata*-elevated dike edge (392.7 m²) and dense *S. alterniflora* (238.7 m²), with reduced contribution from sparse/mixed *S. alterniflora*. Losses of *S. patens* in the buffer areas were also concentrated among vegetated classes, particularly from dense *S. alterniflora* (144.5–202.0 m² at Restoration East; 149.8–163.5 m² at Restoration West). Our observations indicate bidirectional exchange between *S. patens* and *S. alterniflora* and between *S. patens* and *S. pectinata* at both sites along *S. patens* patch boundaries. Losses of *S. patens* to non-vegetated classes were limited. Direct expansion into mud was minor at both sites, indicating that change adjacent to *S. patens* core patches was due to vegetation replacement rather than colonization of exposed substrate. When aggregated across land cover classes, *S. patens* gains exceeded losses during both yearly intervals at both sites (Figure S3). Net expansion was greater at Restoration East, while Restoration West showed a similar pattern with lower and more variable change.

Image-derived predictors responsible for discriminating foundational *Spartina* classes

Welch's *t* statistics identified consistent differences in predictor variables between *S. patens* and both dense and sparse *S. alterniflora* (Figs. 15–16; Figures S4–S15). Absolute *t* statistics exceeded 20 for many of the highest-ranked predictors, with the strongest individual separations reaching 35. Distributions of values for these image-derived predictors showed generally distinct distributions between the congeneric *Spartina* classes (e.g., Figure S16).

Discrimination between *S. patens* and sparse *S. alterniflora* was supported by a combination of texture features (45%), vegetation indices (33%), and raw reflectance variables (22%) (Fig. 15; Table S23). Considering the original spectral bands contributing to all predictor types, near-infrared (NIR842) and red-edge wavelengths (RedEdge740 and RedEdge717) had the highest mean contribution frequencies across site-year comparisons (Fig. 16). Many of the highest-ranked texture features and vegetation indices were also derived from these wavelengths, indicating that discrimination between *S. patens* and sparse *S. alterniflora* relied primarily on near-infrared and red-edge information regardless of predictor type. The strongest individual separation occurred for August RedEdge740 local mean at Restoration East in 2021 ($|t| = 35.0$), followed closely by August NIR842 local mean ($|t| = 34.4$).

In contrast, discrimination between *S. patens* and dense *S. alterniflora* relied predominantly on texture features (64%) and raw reflectance variables (33%), whereas vegetation indices contributed only 3% of the highest-ranked predictors (Fig. 15; Table S23). The underlying spectral information was distributed across a broader range of wavelengths than in sparse comparisons, with RedEdge717 having the highest mean contribution frequency, followed by blue, green, and near-infrared bands (Fig. 16). The strongest individual separation occurred for August RedEdge717 local mean at Restoration East in 2022 ($|t| = 32.2$).

Across all site-year combinations, late-season imagery consistently provided the greatest discriminatory power (Table S23). August imagery accounted for 75% of the highest-ranked predictors distinguishing *S. patens* from dense *S. alterniflora*, whereas August (60%) and July (38%) together accounted for nearly all of the highest-ranked predictors distinguishing *S. patens* from sparse *S. alterniflora*. Among textural features, local mean was by far the most frequently selected metric, representing approximately half of all selected texture predictors in both dense (51%) and sparse (52%) comparisons, with homogeneity, GLDV entropy, entropy, dissimilarity, and GLDV angular second moment occurring less frequently (Table S23). Vegetation indices contributed little to discrimination from dense *S. alterniflora*, but were more important for sparse *S. alterniflora*, where WAVI comprised nearly half (48%) of the selected vegetation indices, followed by GDVI (25%) and DVI (23%).

Discussion

Vegetation trajectories after a decade of restoration

After more than a decade following tidal reconnection, vegetation dynamics at the Aulac restoration sites were dominated by vegetation replacement rather than colonization of bare sediment. Most gains of *Spartina patens* occurred in areas previously occupied by *S. alterniflora*, indicating that species

replacement was a major pathway of vegetation change during this stage of restoration. Although this pattern is consistent with competitive interactions described in salt marsh succession studies (e.g., Bertness, 1991), our observational approach cannot directly identify the mechanisms responsible, and changes in environmental conditions may also have contributed. The spread of *S. patens* within an established *S. alterniflora* matrix indicates progression toward later stages of restoration, where vegetation change occurs via community reorganization and high-marsh development (Virgin et al., 2020). Multi-temporal Sentinel-2 analyses of the same sites similarly detected increases in high-marsh vegetation during this period (Naojee et al., 2024), showing that the trajectory was detectable across multiple spatial scales. In our study, patch trajectory analyses showed areal increases in persistent *S. patens* patches (Fig. 13). This pattern was consistent with field measurements reported by Norris et al. (2022b), where *S. patens* patches exhibited substantial within-season growth over 90 days (~ 3 months). For example, *S. patens* patch area increased by 80–90% over a single growing season in 2020 and 2021, with lower but still notable growth (~ 30%) observed in 2022. Although the two studies operated at different temporal scales (intra- vs. interannual), both indicated sustained *S. patens* spread more than a decade after tidal reconnection. Overall, vegetation changes between 2020 and 2022 involved gradual expansion of *S. patens* and continued shifts between dense and sparse *S. alterniflora*-dominated areas. Similar trajectories have been reported in other restoring salt marshes, where rapid early plant colonization is followed by slower reorganization as marshes mature and vegetation zonation develops (Garbutt et al., 2006; Mossman et al., 2012; Raposa et al., 2016; Wolters et al., 2005).

Underlying processes of high-marsh expansion

Site-wide transition analyses and patch-edge buffers suggested that increases in *S. patens* cover in 2020 – 2022 were associated mostly with expansion of existing patches. At both Aulac restoration sites, gains of *S. patens* occurred predominantly through replacement of adjacent vegetation, particularly *S. alterniflora*, whereas direct colonization of mud by *S. patens* was uncommon. The strong discriminatory ability of near-infrared, red-edge, and texture-derived predictors further suggests that vegetation replacement was associated with measurable differences in canopy structure and spectral characteristics between adjacent *S. patens* and *S. alterniflora* stands. Also, a substantial amount of *S. alterniflora* to *S. patens* transitions occurred within 2 m of established patch edges, indicating that lateral vegetative spread accounted for a large share of observed gains, although gains outside these areas suggested some contribution from new patch establishment. Establishment of *S. patens* independent of patch expansion likely reflects dispersal-driven processes such as ice rafting or hydrological connectivity (Nordio & Fagherazzi, 2023; Rabinowitz et al., 2022; Stopak et al., 2022; Sun et al., 2020). Expansion concentrated along patch boundaries is consistent with self-organizing salt marsh dynamics, where feedbacks among plant growth, sediment trapping, and local hydrodynamics reinforce patch growth and spatial consolidation over time (Kirwan et al., 2016; van Belzen et al., 2017; van de Koppel et al., 2005). In sum, our results indicate that vegetation change in intermediate to later stages of restoration (10 to 12 years after tidal reconnection) is mainly due to lateral expansion and vegetation replacement (likely from interspecific competition) at patch boundaries, highlighting the importance of patch-scale processes during high-marsh development (Norris et al., 2022b).

Insights from differences in site dynamics

Aulac Restoration East and Restoration West exhibited broadly similar vegetation dynamics during the 2020–2022 monitoring period. Both sites showed increasing *S. patens* cover and patch expansion, as well as exchanges between dense and sparse *S. alterniflora* land cover classes (Table 1). At both sites, net transitions between *S. patens* and *S. alterniflora* favored *S. patens*, with conversion of *S. alterniflora* to *S. patens* occurring more frequently than the reverse. Differences between sites were primarily related to the magnitude and timing of these changes rather than their overall direction. For example, transitions between dense and sparse *S. alterniflora* classes were more pronounced at Restoration West, whereas gains of *S. patens* were generally more consistent at Restoration East. These differences may reflect modest variation in environmental conditions and the timing of vegetation development. Established *S. patens* patches were first documented at Restoration West in 2016, whereas comparable patches were not detected at Restoration East until 2020 (Norris et al., 2022b; Stack Mills et al., 2023). Restoration West also began at higher elevation (average of 5.59 m CGVD28 in the west site vs. 5.16 m in the east site, in 2010), while Restoration East experienced greater sediment deposition following tidal reconnection (average of 11.2 cm vs. 7.6 cm deposition after the first year, in 2011, and 81.8 cm vs. 40.3 cm deposition after 10 years, in 2020, for the east and west sites, respectively; Virgin et al., 2020; J. Ollerhead, unpublished data). By 2021, surface elevation of Restoration East was gaining on that of Restoration West (mean ± SD, n = 18 – 27 measured locations: 5.85 ± 0.20 m in the east site vs. 6.01 ± 0.23 m CGVD28 in the west site; J. Ollerhead, unpublished data); and so, *S. patens* establishment appears to also be catching up. Additionally, small differences in hydrodynamic forcing and nutrient availability can influence vegetation communities (Best et al., 2018; Muench & Elsey-Quirk, 2019; Negrin et al., 2011). Where local conditions cross thresholds suitable for high-marsh persistence, *S. patens* may increasingly replace *S. alterniflora*; elsewhere, vegetation change may be expressed primarily as shifts between dense and sparse *S. alterniflora* states (Norris et al., 2022b). Together, our site-specific observations likely reflect threshold-dependent responses in the salt marsh system (Ganju et al., 2017). The expansion of *S. patens* may also indicate the development of greater elevation capital, potentially increasing resilience to sea-level rise, although evaluating this relationship directly will require continued monitoring of vegetation and elevation change. Despite differences between the sites during earlier stages of restoration, the similarity in vegetation cover and dynamics observed after approximately a decade suggests that both sites are converging toward comparable stages of vegetation development, and that they provide a model for the restoration trajectory of former pasturelands in macrotidal, ice-influenced environments.

Implications of our study for monitoring restoring salt marshes

Based on our study, vegetation changes during later stages of restoration occur through fine-scale patch expansion and species replacement (likely competitive interactions) even where overall composition appears relatively stable. Measuring these processes across an entire marsh using field surveys alone is difficult because changes often occur as subtle reorganization within an already vegetated matrix. High-resolution UAV imagery addressed this limitation by allowing patch boundaries and localized transitions

to be mapped at approximately 7.4-cm spatial resolution (7.4 cm pixel size; approximately 7.4 cm × 7.4 cm on the ground), while multispectral bands, vegetation indices, and texture features supported discrimination among co-occurring vegetation classes. Predictor-importance rankings from the full land-cover RF classifications demonstrated that not all image-derived information contributed equally to vegetation classification. Texture features were consistently prominent, particularly at Restoration East, while models for Restoration West relied on a broader mixture of texture features, vegetation indices, and raw reflectance bands (Figures S1–S2). The targeted analysis of the congeneric *Spartina* grasses further clarified which predictors distinguished these closely related vegetation classes. Differences between *S. patens* and sparse *S. alterniflora* were primarily associated with predictors derived from near-infrared and red-edge wavelengths, either directly through reflectance bands or indirectly through vegetation indices and texture measures. In contrast, discrimination between *S. patens* and dense *S. alterniflora* relied more heavily on texture features derived from a broader combination of visible, red-edge, and near-infrared wavelengths. Together, these findings suggest that the optimal predictor variables depend on the spectral and structural characteristics of the classes being compared. This is consistent with previous studies showing the value of red-edge, near-infrared, and texture-derived information for coastal wetland mapping (Adam et al., 2010; Kim et al., 2023a; Norris et al., 2024), while further demonstrating that the relative importance of these predictor types and spectral bands varies depending on the vegetation classes being distinguished. Pairwise analyses can therefore provide information that is obscured by overall variable-importance rankings and may help guide sensor selection and predictor generation for future monitoring.

The distinction between vegetation classes is particularly important in later stages of salt marsh restoration, when vegetation change increasingly reflects the transition from low-marsh to high-marsh communities rather than colonization of previously unvegetated areas (Roman & Burdick, 2012; Virgin et al., 2020). Our framework is also applicable to earlier stages of marsh development, where vegetation expansion occurs through patch formation and lateral spread across bare sediment (Garbutt et al., 2006; Mossman et al., 2012; Norris et al., 2022b; Wolters et al., 2005). Patch dynamics are typically easier to quantify during earlier restoration stages because contrasts between vegetation and mud are more visually distinct and multispectral information may be less critical for classification. At fully or nearly fully vegetated sites, however, multispectral and multitemporal information becomes increasingly important for distinguishing adjacent vegetation classes. In our targeted analysis of the congeneric *Spartina* grasses, August imagery consistently contributed the largest proportion of top-ranked predictors, while July imagery made an additional contribution to distinguishing *S. patens* from sparse *S. alterniflora*. This pattern suggests that late-season imagery captures phenological differences among marsh vegetation that are less apparent earlier in the growing season. Monitoring programs targeting species with subtle spectral differences should therefore include late-season imagery and, where feasible, multiple acquisition dates that capture seasonal vegetation development.

Fine-scale observations of vegetation patch dynamics also provide empirical data for process-based models of salt marsh restoration. Similar UAV-based approaches have been used to quantify *S. alterniflora* patch growth across environmental gradients in coastal settings (Zhu et al., 2019), while

patch-based analyses have also been applied in ecosystems such as seagrass meadows and terrestrial landscapes (Barrell & Grant, 2015; Zhang et al., 2021). Many eco-geomorphological models simulate marsh development by representing interactions between vegetation dynamics and physical processes such as hydrodynamics, sediment transport, and platform elevation change (Best et al., 2018; Fagherazzi et al., 2012; Wu et al., 2017). Because vegetation expansion in these models is typically represented using simplified rules (D'Alpaos et al., 2007; Kirwan & Murray, 2007), empirical observations of plant patch persistence, lateral expansion, and vegetation replacement derived from UAV imagery would help constrain model parameters and improve representation of vegetation dynamics. Our framework demonstrates that multi-temporal UAV imagery can support restoration monitoring while generating empirical observations of vegetation dynamics that may also be useful for parameterizing and evaluating future models of salt marsh succession.

Limitations and future directions

Several limitations should be considered when interpreting our UAV-based findings and guiding future research. First, spatial uncertainty associated with UAV data collection and classification may influence the delineation of small vegetation patches and the boundaries between adjacent vegetation classes. In our study, field observations and image alignment relied partially on handheld GPS units (~ 3 m accuracy) rather than centimeter-level RTK or PPK positioning. To minimize these effects, we co-registered orthomosaics using stable landscape features prior to classification; however, photogrammetric workflows without survey-grade positioning can still introduce horizontal uncertainty during image alignment and georeferencing (James & Robson, 2014; Turner et al., 2016). Fine-resolution classifications may also be affected by speckle and plant patch boundary instability, introducing uncertainty in patch delineation and potentially exaggerating interannual vegetation change (Maxwell et al., 2018). In our study, we applied patch filtering and minimum-area thresholds to reduce noise; however, classification errors are most likely to occur along boundaries between vegetation types where mixed pixels and gradual transitions reduce spectral separability (Foody, 2002). Nevertheless, the consistent spatial patterns and multi-year trajectories observed across both restoration sites suggest that the observed changes in our study primarily reflect ecological processes rather than classification noise, although boundary uncertainty may still influence the magnitude and location of these patterns. Future work could reduce these uncertainties through RTK-enabled UAV systems, ground control points (GCPs), and UAV-LiDAR platforms, which enable centimeter-scale positioning and improved terrain and vegetation characterization in complex marsh environments (Curcio et al., 2022; Meng et al., 2017; Pinton et al., 2021). Classification approaches that incorporate spatial context, such as object-based image analysis and deep learning, may further improve mapping performance where patch structure is important, although gains relative to pixel-based methods are often context dependent (Norris et al., 2024; Wang et al., 2023).

Second, the temporal scope of the analysis was limited to a three-year period (2020–2022). Although this interval captured measurable expansion of *S. patens* and repeated transitions between dense and sparse/mixed *S. alterniflora* classes, salt marsh restoration trajectories typically unfold over decadal

timescales (Norris et al., 2022b; Roman & Burdick, 2012). As a result, the observed trends may represent short-term variability rather than sustained directional change toward mature high-marsh zonation. Longer-term monitoring using UAV and satellite time series is therefore needed to distinguish transient dynamics from long-term trajectories and to quantify processes such as patch expansion, vegetation migration, and succession (Broussard et al., 2018; Windle et al., 2023). Such datasets would also enable evaluation of the temporal transferability of classification models by testing whether models trained in one year can be reliably applied across subsequent years or different restoration sites, potentially reducing the need for annual retraining while improving understanding of the stability of spectral relationships through time.

Third, the present analysis focused on vegetation dynamics derived from classified imagery and therefore did not directly examine either the environmental controls underlying vegetation change or its ecological consequences. Integrating species-level vegetation maps with elevation models, sediment characteristics (e.g., grain size, organic matter content, bulk density), hydrological metrics, and nutrient availability would help identify the factors driving vegetation distribution, biomass, and marsh development (Balke et al., 2016; Belliard et al., 2017; Negrin et al., 2011). Complementary measurements, such as wave dissipation, soil carbon accumulation, microbial communities, soil chemistry, and nekton use, would then help assess concurrent levels of ecosystem functions and services as the high marsh develops (Kim et al., 2023b; Möller & Spencer, 2002; Weinstein et al., 2019; Wollenberg et al., 2018).

Fourth, plant patch-based analyses were anchored to persistent *S. patens* cores to examine edge-mediated expansion and did not explicitly quantify colonization or establishment of new patches. Because *Spartina* species expand through both clonal growth and establishment of new patches following dispersal and hydrological connectivity (Elsey-Quirk et al., 2009; Sun et al., 2020), our patch-core framework likely underrepresents the role of colonization. Future work should explicitly quantify patch initiation and dispersal processes to better capture the full range of processes underlying marsh vegetation change.

Finally, our pairwise analysis of image-derived predictors targeting congeneric *Spartina* classes was motivated by the need to investigate potential spectral differences between established *S. patens* and *S. alterniflora* seedlings. Early and mid-season young-of-the-year *S. alterniflora* resemble *S. patens* morphologically and may therefore exhibit similar textural features before their stems and blades widen (Norris et al., 2022b; Redfield, 1972). Our restoration sites can have many *S. alterniflora* seedlings under the mature *S. alterniflora* canopy, visible through gaps in this canopy to field observers as well as the UAV. We questioned whether the temporary appearance and subsequent disappearance of nominal *S. patens* (based on the classification, particularly in the northwest half of Restoration East; Fig. 11) was the appearance and subsequent maturing of *S. alterniflora* seedlings. Although our analysis showed differences in raw spectral reflectance between *S. patens* and the mapped *S. alterniflora* classes, it did not explicitly evaluate *S. alterniflora* seedlings. While our study distinguished mature vegetation with high accuracy, evaluating the spectral characteristics and seasonal development of seedlings using the analytical framework developed here would be complementary, and may reduce some of the localized

classification uncertainty. Furthermore, it would provide additional insight into the relative importance of clonal and sexual reproduction modes of vegetation spread (Metcalfe et al., 1986; Silvertown, 2008).

Conclusion

High-resolution multispectral UAV imagery demonstrated that vegetation change at the Aulac restoration sites reflected internal restructuring within an established marsh platform rather than continued colonization of bare substrate. Between 2020 and 2022, *Spartina patens* expanded gradually at both sites, with growth concentrated along the boundaries of stable (core) *S. patens* patches and occurring through replacement of adjacent vegetation, particularly *S. alterniflora*. These patterns indicate a later stage of marsh development characterized by patch expansion, vegetation replacement, community reorganization, and high-marsh establishment. Monitoring these dynamics provides insight into high-marsh development that is not captured by changes in overall vegetation composition alone. By combining pixel-based UAV classifications with plant patch-based analyses and targeted analyses of image-derived predictors, our study provides a transferable methodological framework for quantifying vegetation change in fully vegetated salt marshes and linking fine-scale patch dynamics to restoration trajectories. Ecologically, our study provides the first whole-site and detailed quantification of *S. patens* expansion and so establishes a foundation for future assessments of how vegetation change influences ecosystem functions and services as restoring marshes mature.

Declarations

Ethics approval and consent to participate

Not applicable.

Consent for publication

Not applicable.

Authors' contributions

Conceptualization, G.S.N., B.L., A.L., M.A.B., and A.R.H.; methodology, G.S.N., B.L., A.L., and M.A.B.; formal analysis, G.S.N.; investigation, G.S.N.; resources, B.L., A.L., and M.A.B.; data curation, G.S.N.; writing—original draft preparation, G.S.N.; writing—review and editing, G.S.N., M.A.B., B.L., A.R.H., visualization, G.S.N.; supervision, M.A.B., B.L., and A.L.; project administration, G.S.N., M.A.B., B.L., and A.L.; funding acquisition, G.S.N., B.L., M.A.B., and A.L. All authors have read and agreed to the published version of the manuscript.

Acknowledgements

We thank Swarna Naojee, Eleanor Gallant, Olivia Hanson, Kiana Endresz, Jonathan Linihan, Alexa Stack Mills, Elizabeth Bateman, Emily McCoy, Krish Thapar, Eke Kalu, Anajose Reyes-Guevara, Julianne Richard, Matthew Mogle, Lyle Vicaire, Jenna Watson, Nolan Doak, Morgan Richard, and Angelica Whiteway for assisting in the field, and Jeff Ollerhead for providing marsh surface elevation and sediment deposition data. We also thank Jeff Ollerhead, Chris Wong, Olivier Grimard, Ata Haddadi, and Nic McLellan for useful discussion and feedback.

Availability of data and material

The datasets used during the present study are available from the corresponding author upon request.

Competing interests

The authors declare no conflicts of interest. The funders had no role in the design of the study; in the collection, analyses, or interpretation of data; in the writing of the manuscript; or in the decision to publish the results.

Funding

Funding for the project was from Ducks Unlimited Canada, NB Department of Transportation and Infrastructure, Fisheries and Oceans Canada (Small Craft Harbours), the New Brunswick Environmental Trust Fund (Project #200133, #210235, #220335 grants to AL, BL, MAB, GSN), MITACS ACCELERATE Internship (GSN, MAB) and Doctoral Fellowship (GSN, MAB, BL) with Ducks Unlimited Canada as the partner, the Natural Sciences and Engineering Research Council of Canada (NSERC; Discovery grants to BL and MAB, and CREATE grants to BL), New Brunswick Innovation Fund (NBIF; Emerging Projects grant to BL and MAB, and Research Assistantships Initiative grant to BL), the Career Launcher Program administered by Colleges and Institutes Canada (Clean Tech Internships via Environment and Climate Change Canada, and Natural Resources Internship via Natural Resources Canada), the Canada Summer Jobs Program (Employment and Social Development Canada), New Brunswick SEED Co-op Program (New Brunswick Post-Secondary Education, Training and Labour) in 2020 and Future NB Co-op in 2021 along with the UNB Engineering and Science Co-op Program, and the University of New Brunswick (UNB).

References

1. Aasen H, Burkart A, Bolten A, Bareth G (2015) Generating 3D hyperspectral information with lightweight UAV snapshot cameras for vegetation monitoring: From camera calibration to quality assurance. ISPRS J Photogrammetry Remote Sens 108:245–259. https://doi.org/10.1016/j.isprsjprs.2015.08.002
2. Adam E, Mutanga O, Rugege D (2010) Multispectral and hyperspectral remote sensing for identification and mapping of wetland vegetation: A review. Wetlands Ecol Manage 18(3):281–296.

https://doi.org/10.1007/s11273-009-9169-z

3. Adams JB, Raw JL, Riddin T, Wasserman J, Van Niekerk L (2021) Salt marsh restoration for the provision of multiple ecosystem services. Diversity 13(12):680. https://doi.org/10.3390/d13120680
4. Alvarez-Vanhard E, Corpetti T, Houet T (2021) UAV & satellite synergies for optical remote sensing applications: A literature review. Sci Remote Sens 3:100019. https://doi.org/10.1016/j.srs.2021.100019
5. Angelini C, Altieri AH, Silliman BR, Bertness MD (2011) Interactions among foundation species and their consequences for community organization, biodiversity, and conservation. Bioscience 61(10):782–789. https://doi.org/10.1525/bio.2011.61.10.8
6. Baker R, Taylor MD, Able KW, Beck MW, Cebrian J, Colombano DD, Connolly RM, Currin C, Deegan LA, Feller IC, Gilby BL, Kimball ME, Minello TJ, Rozas LP, Simenstad C, Turner RE, Waltham NJ, Weinstein MP, Ziegler SL, zu Ermgassen PSE, Alcott C, Alford SB, Barbeau MA, Crosby SC, Dodds K, Frank A, Goeke J, Goodridge Gaines LA, Hardcastle FE, Henderson CJ, James WR, Kenworthy MD, Lesser J, Mallick D, Martin CW, McDonald AE, McLuckie C, Morrison BH, Nelson JA, Norris GS, Ollerhead J, Pahl J, Ramsden S, Rehage JS, Reinhardt J, Rezek R, Risse LM (2020) Fisheries rely on threatened salt marshes. Science 370:670–671 J. A. M. Smith, E. L. Sparks, & L. W. Staver
7. Balke T, Stock M, Jensen K, Bouma TJ, Kleyer M (2016) A global analysis of the seaward salt marsh extent: The importance of tidal range. Water Resour Res 52(5):3775–3786. https://doi.org/10.1002/2015WR018318
8. Barbier EB, Hacker SD, Kennedy C, Koch EW, Stier AC, Silliman BR (2011) The value of estuarine and coastal ecosystem services. Ecol Monogr 81(2):169–193. https://doi.org/10.1890/10-1510.1
9. Barrell J, Grant J (2015) High-resolution, low-altitude aerial photography in physical geography: A case study characterizing eelgrass (*Zostera marina*) and blue mussel (*Mytilus edulis*) landscape mosaic structure. Prog Phys Geogr 39(4):440–459. https://doi.org/10.1177/0309133315578943
10. Belgiu M, Drăguţ L (2016) Random forest in remote sensing: A review of applications and future directions. ISPRS J Photogrammetry Remote Sens 114:24–31. https://doi.org/10.1016/j.isprsjprs.2016.01.011
11. Belliard JP, Temmerman S, Toffolon M (2017) Ecogeomorphic relations between marsh surface elevation and vegetation properties in a temperate multi-species salt marsh. Earth Surf Proc Land 42(6):855–865. https://doi.org/10.1002/esp.4041
12. Bertness MD (1991) Zonation of *Spartina patens* and *Spartina alterniflora* in New England salt marsh. Ecology 72(1):138–148. https://doi.org/10.2307/1938909
13. Bertness MD, Ellison AM (1987) Determinants of pattern in a New England salt marsh plant community. Ecol Monogr 57(2):129–147. https://doi.org/10.2307/1942621
14. Best ÜSN, van der Wegen M, Dijkstra J, Willemsen PWJM, Borsje BW, Roelvink D (2018) Do salt marshes survive sea-level rise? Modelling wave action, morphodynamics and vegetation dynamics. Environ Model Softw 109:152–166. https://doi.org/10.1016/j.envsoft.2018.08.004

15. Blaschke T (2010) Object based image analysis for remote sensing. ISPRS J Photogrammetry Remote Sens 65(1):2–16. https://doi.org/10.1016/j.isprsjprs.2009.06.004
16. Boone LK, Ollerhead J, Barbeau MA, Beck AD, Sanderson BG, McLellan NR (2017) Returning the tide to dikelands in a macrotidal and ice-influenced environment: Challenges and lessons learned. In C. W. Finkl & C. Makowski (Eds.), *Coastal wetlands: Alteration and remediation*(Coastal Research Library, Vol. 21, pp. 705–749). Springer. https://doi.org/10.1007/978-3-319-56179-0_21
17. Bortolus A, Adam P, Adams JB, Ainouche ML, Ayres D, Bertness MD, Zhou H (2019) Supporting *Spartina*: Interdisciplinary perspective shows *Spartina* as a distinct solid genus. Ecology 100(11):e02863. https://doi.org/10.1002/ecy.2863
18. Bouchard V, Lefeuvre JC (2000) Primary production and macro-detritus dynamics in a European salt marsh: Carbon and nitrogen budgets. Aquat Bot 67(1):23–42. https://doi.org/10.1016/S0304-3770(99)00086-8
19. Bowron TM, Neatt N, van Proosdij D, Lundholm J (2012) Salt marsh tidal restoration in Canada's maritime provinces. In: Roman CT, Burdick DM (eds) Tidal marsh restoration: A synthesis of science and management. Island, pp 191–209
20. Breiman L (2001) Random forests. Mach Learn 45(1):5–32. https://doi.org/10.1023/A:1010933404324
21. Broussard W, Suir G, Visser J (2018) Unmanned aircraft systems (UAS) and satellite imagery collections in a coastal intermediate marsh to determine vegetation and land-water interface. U.S. Army Engineer Research and Development Center. https://doi.org/10.21079/11681/29517
22. Cahoon DR, Lynch JC, Roman CT, Schmit JP, Skidds DE (2019) Evaluating the relationship among wetland vertical development, elevation capital, sea-level rise and tidal marsh sustainability. Estuaries Coasts 42(1):1–15. https://doi.org/10.1007/s12237-018-0448-x
23. Cahoon DR, McKee KL, Morris JT (2021) How plants influence resilience of salt marsh and mangrove wetlands to sea-level rise. Estuaries Coasts 44(4):883–898. https://doi.org/10.1007/s12237-020-00834-w
24. Colombano DD, Litvin SY, Ziegler SL, Alford SB, Baker R, Barbeau MA, Cebrian J, Connolly RM, Deegan LA, Lesser JS, Martin CW, McDonald AE, McLuckie C, Morrison BH, Pahl JW, Risse LM, Smith JAM, Staver LW, Turner RE, Waltham NJ, Ziegler SL (2021) Climate change implications for tidal marshes and food web linkages to estuarine and coastal nekton. Estuaries Coasts 44(6):1637–1648. https://doi.org/10.1007/s12237-020-00891-1
25. Congalton RG, Green K (2009) Assessing the accuracy of remotely sensed data: Principles and practices, 2nd edn. CRC
26. Curcio AC, Peralta G, Aranda M, Barbero L (2022) Evaluating the performance of high spatial resolution UAV-photogrammetry and UAV-LiDAR for salt marshes. Remote Sens 14(15):3582. https://doi.org/10.3390/rs14153582
27. Curcio AC, Barbero L, Peralta G (2024) Enhancing salt marsh monitoring: Estimating biomass with drone-derived habitat-specific models. Remote Sens Applications: Soc Environ 35:101216.

https://doi.org/10.1016/j.rsase.2024.101216

28. D'Alpaos A, Lanzoni S, Marani M, Rinaldo A (2007) Landscape evolution in tidal embayments: Modeling the interplay of erosion, sedimentation, and vegetation dynamics. J Geophys Research: Earth Surf 112:F01008. https://doi.org/10.1029/2006JF000537
29. De Lauretis S, De Battisti D, Grasselli F, Airoldi L (2026) A global review of salt marsh restoration: Why simpler, context-specific strategies can outperform complex approaches. Glob Change Biol 32(5):e70925. https://doi.org/10.1111/gcb.70925
30. Desplanque C, Mossman D (2004) Tides and their seminal impact on the geology, geography, history, and socio-economics of the Bay of Fundy, eastern Canada. Atlantic Geol 40:1–130. https://doi.org/10.4138/729
31. Doughty CL, Cavanaugh KC (2019) Mapping coastal wetland biomass from high-resolution unmanned aerial vehicle imagery. Remote Sens 11(5):540. https://doi.org/10.3390/rs11050540
32. Dronova I, Kislik C, Dinh Z, Kelly M (2021) A review of unoccupied aerial vehicle use in wetland applications: Emerging opportunities in approach, technology, and data. Drones 5(2):45. https://doi.org/10.3390/drones5020045
33. Elsey-Quirk T, Middleton BA, Proffitt CE (2009) Seed dispersal and seedling emergence in a created and a natural salt marsh on the Gulf of Mexico coast in southwest Louisiana. U S Restor Ecol 17(5):688–697. https://doi.org/10.1111/j.1526-100X.2008.00398.x
34. Fagherazzi S, Kirwan ML, Mudd SM, Guntenspergen GR, Temmerman S, D'Alpaos A, van de Koppel J, Rybczyk JM, Reyes E, Craft C, Clough J (2012) Numerical models of salt marsh evolution: Ecological, geomorphic, and climatic factors. Rev Geophys 50:RG1002. https://doi.org/10.1029/2011RG000359
35. Fisheries and Oceans Canada (2026) *Tides, currents, and water levels*. Retrieved February 21, 2026, from https://www.tides.gc.ca/en/stations/190
36. Foody GM (2002) Status of land cover classification accuracy assessment. Remote Sens Environ 80(1):185–201. https://doi.org/10.1016/S0034-4257(01)00295-4
37. Gallant K, Withey P, Risk D, Van Kooten GC, Spafford L (2020) Measurement and economic valuation of carbon sequestration in Nova Scotian wetlands. Ecol Econ 171:106619. https://doi.org/10.1016/j.ecolecon.2020.106619
38. Ganju NK, Defne Z, Kirwan ML, Fagherazzi S, D'Alpaos A, Carniello L (2017) Spatially integrative metrics reveal hidden vulnerability of microtidal salt marshes. Nat Commun 8:14156. https://doi.org/10.1038/ncomms14156
39. Garbutt A, Reading CJ, Wolters M, Gray AJ, Rothery P (2006) Monitoring the development of intertidal habitats on former agricultural land after managed realignment. Mar Pollut Bull 53:162–173. https://doi.org/10.1016/j.marpolbul.2005.09.015
40. Garzon JL, Maza M, Ferreira CM, Lara JL, Losada IJ (2019) Wave attenuation by *Spartina* saltmarshes in the Chesapeake Bay under storm surge conditions. J Geophys Research: Oceans 124(8):5220–5243. https://doi.org/10.1029/2018JC014865

41. Gedan KB, Kirwan ML, Wolanski E, Barbier EB, Silliman BR (2011) The present and future role of coastal wetland vegetation in protecting shorelines: Answering recent challenges to the paradigm. Clim Change 106(1):7–29. https://doi.org/10.1007/s10584-010-0003-7
42. Guo Q, Liu J, Li Y, Zhai Q, Wang Y, Wu F, Hu T, Wan H, Liu H, Shen W (2016) A near-surface remote sensing platform for biodiversity monitoring: Perspectives and prospects. Biodivers Sci 24(11):1249–1266. https://doi.org/10.17520/biods.2016059
43. Haralick RM, Shanmugam K, Dinstein I (1973) Textural features for image classification. *IEEE Transactions on Systems, Man, and Cybernetics, SMC-3*(6), 610–621. https://doi.org/10.1109/TSMC.1973.4309314
44. Haskins J, Endris C, Thomsen AS, Gerbl F, Fountain MC, Wasson K (2021) UAV to inform restoration: A case study from a California tidal marsh. Front Environ Sci 9:642906. https://doi.org/10.3389/fenvs.2021.642906
45. Huang Y, Lu C, Jia M, Wang Z, Su Y, Su Y (2023) Plant species classification of coastal wetlands based on UAV images and object-oriented deep learning. Biodivers Sci 31:22411. https://doi.org/10.17520/biods.2022411
46. James MR, Robson S (2014) Mitigating systematic error in topographic models derived from UAV and ground-based image networks. Earth Surf Proc Land 39(10):1413–1420. https://doi.org/10.1002/esp.3609
47. Kim K, Lee D, Jang Y, Lee J, Kim CH, Jou HT, Ryu J (2023a) Deep learning of high-resolution unmanned aerial vehicle imagery for classifying halophyte species. Remote Sens 15(11):2723. https://doi.org/10.3390/rs15112723
48. Kim C, Staver LW, Chen X, Bulseco A, Cornwell JC, Malkin SY (2023b) Microbial community succession along a chronosequence in constructed salt marsh soils. Microb Ecol 85(3):931–950. https://doi.org/10.1007/s00248-023-02189-8
49. Kirwan ML, Murray AB (2007) A coupled geomorphic and ecological model of tidal marsh evolution. *Proceedings of the National Academy of Sciences, 104*(15), 6118–6122. https://doi.org/10.1073/pnas.0700958104
50. Kirwan ML, Megonigal JP (2013) Tidal wetland stability in the face of human impacts and sea-level rise. Nature 504:53–60. https://doi.org/10.1038/nature12856
51. Kirwan ML, Temmerman S, Skeehan EE, Guntenspergen GR, Fagherazzi S (2016) Overestimation of marsh vulnerability to sea level rise. Nat Clim Change 6:253–260. https://doi.org/10.1038/nclimate2909
52. Klemas V (2013) Remote sensing of coastal wetland biomass: An overview. J Coastal Res 290:1016–1028. https://doi.org/10.2112/JCOASTRES-D-12-00237.1
53. Li C, Zhou L, Xu W (2021) Estimating aboveground biomass using Sentinel-2 MSI data and ensemble algorithms for grassland in the Shengjin Lake wetland, China. Remote Sens 13(8):1595. https://doi.org/10.3390/rs13081595
54. Liaw A, Wiener M (2002) Classification and regression by randomForest. R News 2(3):18–22

55. Maxwell AE, Warner TA, Fang F (2018) Implementation of machine-learning classification in remote sensing: An applied review. Remote Sens 10(9):153. https://doi.org/10.3390/rs10091533
56. Martínez Prentice R, Villoslada Peciña M, Ward RD, Bergamo TF, Joyce CB, Sepp K (2021) Machine learning classification and accuracy assessment from high-resolution images of coastal wetlands. Remote Sens 13(18):3669. https://doi.org/10.3390/rs13183669
57. Meng X, Shang N, Zhang X, Li C, Zhao K, Qiu X, Weeks E (2017) Photogrammetric UAV mapping of terrain under dense coastal vegetation: An object-oriented classification ensemble algorithm for classification and terrain correction. Remote Sens 9(11):1187. https://doi.org/10.3390/rs9111187
58. Metcalfe WS, Ellison AM, Bertness MD (1986) Survivorship and spatial development of *Spartina alterniflora* Loisel. (Gramineae) seedlings in a New England salt marsh. Ann Botany 58(2):249–258. https://doi.org/10.1093/oxfordjournals.aob.a087202
59. Millard K, Redden AM, Webster T, Stewart H (2013) Use of GIS and high resolution LiDAR in salt marsh restoration site suitability assessments in the Upper Bay of Fundy, Canada. Wetlands Ecol Manage 21:243–262. https://doi.org/10.1007/s11273-013-9303-9
60. Möller I, Spencer T (2002) Wave dissipation over macro-tidal saltmarshes: Effects of marsh edge typology and vegetation change. J Coastal Res Special Issue 36:506–521. https://doi.org/10.2112/1551-5036-36.sp1.506
61. Morris JT, Sundareshwar PV, Nietch CT, Kjerfve B, Cahoon DR (2002) Responses of coastal wetlands to rising sea level. Ecology 83:2869–2877. https://doi.org/10.1890/0012-9658(2002)083[2869:ROCWTR]2.0.CO;2
62. Mossman HL, Davy AJ, Grant A (2012) Does managed coastal realignment create saltmarshes with equivalent ecological function? J Appl Ecol 49:1446–1456. https://doi.org/10.1111/j.1365-2664.2012.02198.x
63. Muench A, Elsey-Quirk T (2019) Competitive reversal between plant species is driven by species-specific tolerance to flooding stress and nutrient acquisition during early marsh succession. J Appl Ecol 56:2263–2274. https://doi.org/10.1111/1365-2664.13458
64. Naojee SM, LaRocque A, Leblon B, Norris GS, Barbeau MA, Rowland M (2024) Monitoring saltmarsh restoration in the Upper Bay of Fundy using multi-temporal Sentinel-2 imagery and random forests classifier. Remote Sens 16:4667. https://doi.org/10.3390/rs16244667
65. Nardin W, Taddia Y, Quitadamo M, Vona I, Corbau C, Franchi G, Staver L, Pellegrinelli A (2021) Seasonality and characterization mapping of restored tidal marsh by NDVI imageries coupling UAVs and multispectral camera. Remote Sens 13:4207. https://doi.org/10.3390/rs13214207
66. Negrin V, Spetter C, Asteasuain R, Perillo GME, Marcovecchio JE (2011) Influence of flooding and vegetation on carbon, nitrogen, and phosphorus dynamics in the pore water of a *Spartina alterniflora* salt marsh. J Environ Sci 23(2):212–221. https://doi.org/10.1016/S1001-0742(10)60395-6
67. Nordio G, Fagherazzi S (2023) Recovery of salt marsh vegetation after ice rafting. Mar Ecol Prog Ser 710:57–72. https://doi.org/10.3354/meps14294

68. Norris GS, LaRocque A, Leblon B, Barbeau MA, Hanson AR (2024) Comparing pixel- and object-based approaches for classifying multispectral drone imagery of a salt marsh restoration and reference site. Remote Sens 16:1049. https://doi.org/10.3390/rs16061049
69. Norris GS, Leblon B, LaRocque A, Barbeau MA, Hanson AR (2022a) Effect of textural features for landcover classification of UAV multispectral imagery of a salt marsh restoration site. *The International Archives of the Photogrammetry, Remote Sensing and Spatial Information Sciences, XLIII-B3-2022*, 951–958. https://doi.org/10.5194/isprs-archives-XLIII-B3-2022-951-2022
70. Norris GS, Virgin SDS, Schneider DW, McCoy EM, Wilson JM, Morrill KL, Hayter L, Hicks ME, Barbeau MA (2022b) Patch-level processes of vegetation underlying site-level restoration patterns in a megatidal salt marsh. Front Ecol Evol 10:1000075. https://doi.org/10.3389/fevo.2022.1000075
71. Olofsson P, Foody GM, Herold M, Stehman SV, Woodcock CE, Wulder MA (2014) Good practices for estimating area and assessing accuracy of land change. Remote Sens Environ 148:42–57. https://doi.org/10.1016/j.rse.2014.02.015
72. Ooi SK, Barry A, Lawrence BA, Elphick CS, Helton AM (2022) Vegetation zones as indicators of denitrification potential in salt marshes. Ecol Appl 32(6):e2630. https://doi.org/10.1002/eap.2630
73. Pennings SC, Callaway RM (1992) Salt marsh plant zonation: The relative importance of competition and physical factors. Ecology 73:681–690. https://doi.org/10.2307/1940774
74. Peterson PM, Romaschenko K, Arrieta YH, Saarela JM (2014) A molecular phylogeny and new subgeneric classification of *Sporobolus* (Poaceae: Chloridoideae: Sporobolinae). Taxon 63(6):1212–1243. https://doi.org/10.12705/636.19
75. Pinton D, Canestrelli A, Wilkinson B, Ifju P, Ortega A (2021) Estimating ground elevation and vegetation characteristics in coastal salt marshes using UAV-based LiDAR and digital aerial photogrammetry. Remote Sens 13:4506. https://doi.org/10.3390/rs13224506
76. R Core Team (2025) R: A language and environment for statistical computing. R Foundation for Statistical Computing, Vienna, Austria
77. Rabinowitz TRM, Greene L, Glogowski AD, Bowron T, van Proosdij D, Lundholm JT (2022) Hitchhiking halophytes in wrack and sediment-laden ice blocks contribute to tidal marsh development in the Upper Bay of Fundy. Wetlands Ecol Manage 30(3):375–388. https://doi.org/10.1007/s11273-022-09867-3
78. Raposa KB, Wasson K, Smith E, Crooks JA, Delgado P, Fernald SH, Ferner MC, Helms A, Hice LA, Mora JW, Puckett BJ, Sanger DM, Shull S, Spurrier CS, Stevens R, Lerberg SB, Simenstad CA (2016) Assessing tidal marsh restoration performance using a multimetric approach. Estuaries Coasts 39(3):868–880. https://doi.org/10.1007/s12237-015-9997-x
79. Redfield AC (1972) Development of a New England salt marsh. Ecol Monogr 42(2):201–237. https://doi.org/10.2307/1942263
80. Richardson AJ, Wiegand CL (1977) Distinguishing vegetation from soil background information. Photogram Eng Remote Sens 43(12):1541–1552

81. Roberts DR, Bahn V, Ciuti S, Boyce MS, Elith J, Guillera-Arroita G, Hauenstein S, Lahoz-Monfort JJ, Schröder B, Thuiller W, Warton DI, Wintle BA, Hartig F, Dormann CF (2017) Cross-validation strategies for data with temporal, spatial, hierarchical, or phylogenetic structure. Ecography 40(8):913–929. https://doi.org/10.1111/ecog.02881
82. Roman CT, Burdick DM (eds) (2012) Tidal marsh restoration: A synthesis of science and management. Island. https://doi.org/10.5822/978-1-61091-229-7
83. Rouse JW, Haas RH, Schell JA, Deering DW, Harlan JC (1974) *Monitoring the vernal advancement and retrogradation (green wave effect) of natural vegetation*(NASA/GSFC Type IIIFinal Report). NASA Goddard Space Flight Center
84. Routhier MR, Moore G, Rock B (2023) Assessing spectral band, elevation, and collection date combinations for classifying salt marsh vegetation with UAV imagery. Remote Sens 15:5076. https://doi.org/10.3390/rs15205076
85. Rozas LP (1995) Hydroperiod and its influence on nekton use of the salt marsh: A pulsing ecosystem. Estuaries 18(4):579–590
86. Shawler JL, Ostojic A, Schad A, Macon C, Harwood J (2025) Trade-offs between field and remote geomorphic monitoring of coastal marsh restoration sites: Examples and practical guidance from Coastal Louisiana, USA. Louisiana State University. https://doi.org/10.21079/11681/49876
87. Silvertown J (2008) The evolutionary maintenance of sexual reproduction: Evidence from the ecological distribution of asexual reproduction in clonal plants. Int J Plant Sci 169(1):157–168. https://doi.org/10.1086/523357
88. Stack Mills AME, Norris GS, Barbeau MA (2023) *Dynamics of Spartina patens patches during the 11th and 12th years of salt marsh restoration in Aulac, New Brunswick*(Unpublished technical report). Department of Biology, University of New Brunswick
89. Stopak SR, Smith SM, Kirwan ML, Guntenspergen GR (2022) Quantifying the importance of ice-rafted debris to salt marsh sediment budgets using remote sensing. Remote Sens 14(21):5499. https://doi.org/10.3390/rs14215499
90. Sun L, Shao D, Xie T, Gao W, Ma X, Ning Z, Cui B (2020) How does *Spartina alterniflora* invade in salt marsh in relation to tidal channel networks? Patterns and processes. Remote Sens 12(18):2983. https://doi.org/10.3390/rs12182983
91. Taddia Y, Pellegrinelli A, Corbau C, Franchi G, Staver L, Stevenson J, Nardin W (2021) High-resolution monitoring of tidal systems using UAV: A case study on Poplar Island, MD (USA). Remote Sens 13:1364. https://doi.org/10.3390/rs13071364
92. Thomsen A, Krause J, Appiano M, Tanner K, Endris C, Haskins J, Watson E, Woolfolk A, Fountain M, Wasson K (2021) Monitoring vegetation dynamics at a tidal marsh restoration site: Integrating field methods, remote sensing and modeling. Estuaries Coasts 45:523–538. https://doi.org/10.1007/s12237-021-00977-4
93. Turner D, Lucieer A, Wallace L (2016) Direct georeferencing of ultrahigh-resolution UAV imagery. IEEE Trans Geosci Remote Sens 54(5):2738–2745. https://doi.org/10.1109/TGRS.2013.2265295

94. Turpie KR (2013) Explaining the spectral red-edge features of inundated marsh vegetation. J Coastal Res 29(5):1111–1117. https://doi.org/10.2112/JCOASTRES-D-12-00209.1
95. van Belzen J, van de Koppel J, Kirwan ML, van der Wal D, Herman PMJ, Dakos V, Kéfi S, Scheffer M (2017) Vegetation recovery in tidal marshes reveals critical slowing down under increased inundation. Nat Commun 8:15811. https://doi.org/10.1038/ncomms15811
96. van de Koppel J, van der Wal D, Bakker JP, Herman PMJ (2005) Self-organization and vegetation collapse in salt marsh ecosystems. Am Nat 165(1):E1–E12. https://doi.org/10.1086/426602
97. van Proosdij D, Graham J, Lemieux B, Bowron T, Poirier E, Kickbush J, Ellis K, Lundholm J (2023) High sedimentation rates lead to rapid vegetation recovery in tidal brackish wetland restoration. Front Ecol Evol 11:1112284. https://doi.org/10.3389/fevo.2023.1112284
98. Virgin SDS, Beck AD, Boone LK, Dykstra AK, Ollerhead J, Barbeau MA, McLellan NR (2020) A managed realignment in the Upper Bay of Fundy: Community dynamics during salt marsh restoration over 8 years in a megatidal, ice-influenced environment. Ecol Eng 149:105713. https://doi.org/10.1016/j.ecoleng.2020.105713
99. Waltham NJ, Alcott C, Barbeau MA, Cebrian J, Connolly RM, Deegan LA, Dodds K, Goodridge Gaines LA, Gilby BL, Henderson CJ, McLuckie CM, Minello TJ, Norris GS, Ollerhead J, Pahl J, Reinhardt JF, Rezek RJ, Simenstad CA, Smith JAM, Sparks EL, Staver LW, Ziegler SL, Weinstein MP (2021) Tidal marsh restoration optimism in a changing climate and urbanizing seascape. Estuaries Coasts 44:1681–1690. https://doi.org/10.1007/s12237-020-00875-1
100. Wang C, Morgan GR, Morris JT (2023) Drone LiDAR deep learning for fine-scale bare earth surface and 3D marsh mapping in intertidal estuaries. Sustainability 15(22):15823. https://doi.org/10.3390/su152215823
101. Wasson K, Ganju NK, Defne Z, Endris C, Elsey-Quirk T, Thorne KM, Freeman CM, Guntenspergen G, Nowacki DJ, Raposa KB (2019) Understanding tidal marsh trajectories: Evaluation of multiple indicators of marsh persistence. Environ Res Lett 14(12):124073. https://doi.org/10.1088/1748-9326/ab5a94
102. Weinstein MP, Hazen R, Litvin SY (2019) Response of nekton to tidal salt marsh restoration: A meta-analysis of restoration trajectories. Wetlands 39(3):575–585. https://doi.org/10.1007/s13157-018-1106-6
103. Welch BL (1947) The generalization of Student's problem when several different population variances are involved. Biometrika 34(1–2):28–35. https://doi.org/10.1093/biomet/34.1-2.28
104. Windle AE, Staver L, Elmore A, Scherer S, Keller S, Malmgren B, Silsbe G (2023) Multi-temporal high-resolution marsh vegetation mapping using unoccupied aircraft system remote sensing and machine learning. Front Remote Sens 4. https://doi.org/10.3389/frsen.2023.1140999
105. Wollenberg JT, Ollerhead J, Chmura GL (2018) Rapid carbon accumulation following managed realignment on the Bay of Fundy. PLoS ONE 13(3):e0193930. https://doi.org/10.1371/journal.pone.0193930

106. Wolters M, Garbutt A, Bakker JP (2005) Salt-marsh restoration: Evaluating the success of de-embankments in north-west Europe. Biol Conserv 123:249–268. https://doi.org/10.1016/j.biocon.2004.11.013

107. Wu G, Li H, Liang B, Shi F, Kirby J, Mieras R (2017) Subgrid modeling of salt marsh hydrodynamics with effects of vegetation and vegetation zonation. Earth Surf Proc Land 42:1755–1768. https://doi.org/10.1002/esp.4121

108. Zhang J, Karl JW, Zhou B, Okin GS (2021) UAV-derived imagery for vegetation structure estimation in rangelands. Ecosphere 12:e03830. https://doi.org/10.1002/ecs2.3830

109. Zhu X, Meng L, Zhang Y, Weng Q, Morris J (2019) Tidal and meteorological influences on the growth of invasive *Spartina alterniflora*: Evidence from UAV remote sensing. Remote Sens 11(10):1208. https://doi.org/10.3390/rs11101208

110. Ziegler SL, Baker R, Able KW, Alcott C, Barbeau MA, Beck MW, Cebrian J, Colombano DD, Connolly RM, Currin C, Deegan LA, Feller IC, Gilby BL, Kimball ME, Minello TJ, Rozas LP, Simenstad CA, Turner RE, Waltham NJ, Weinstein MP,zu, Ermgassen PSE (2021) Geographic variation in salt marsh structure and function for nekton: A global synthesis. *Estuaries and Coasts, 44*(6), 1497–1507. https://doi.org/10.1007/s12237-020-00894-y

Figures

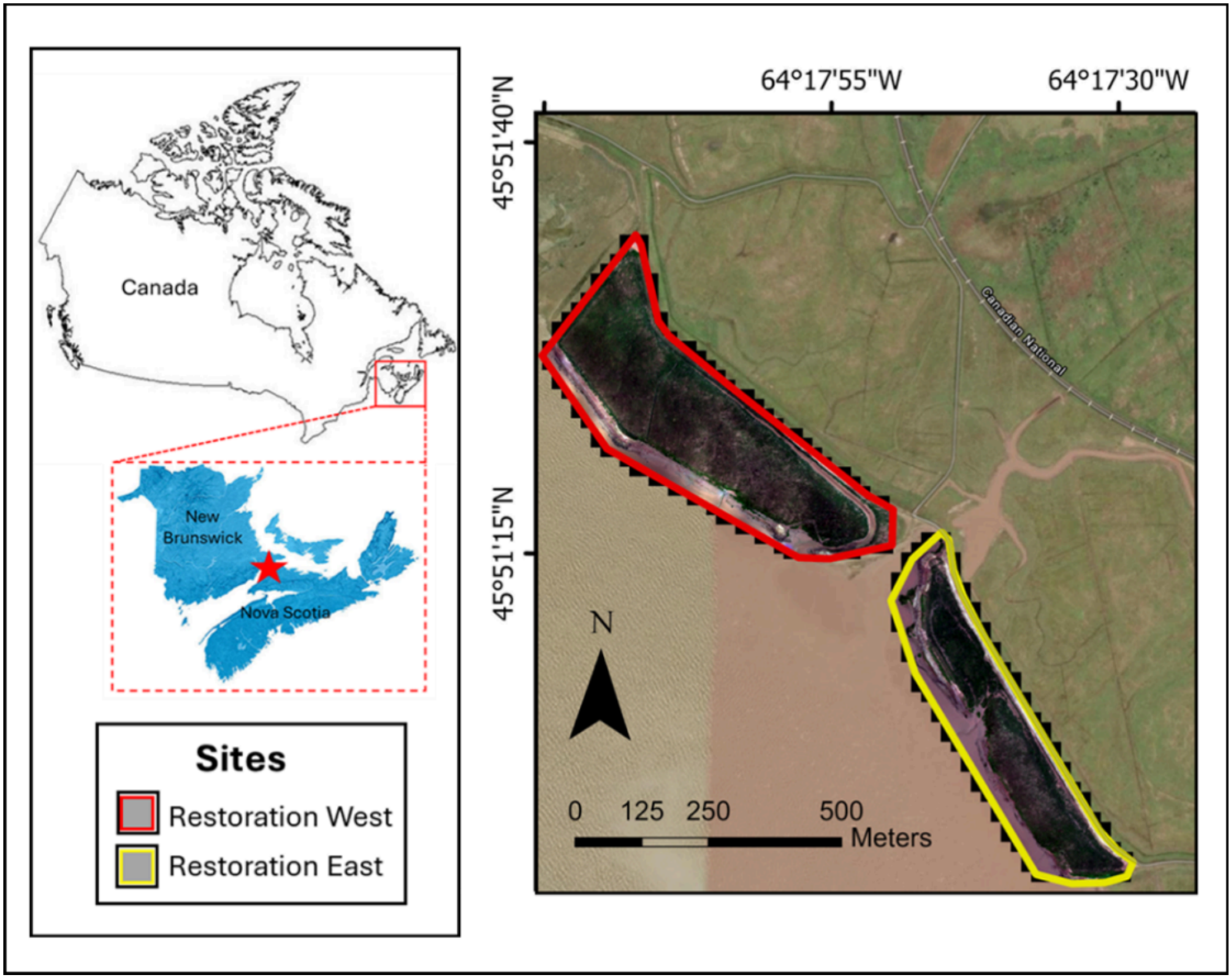

Figure 1

Location of the two salt marsh restoration sites (Restoration West and Restoration East) in Aulac, New Brunswick, monitored using multispectral drone imagery from 2020 to 2022. The right panel shows site boundaries within the Bay of Fundy region, New Brunswick, Canada, while the left panel provides regional context.

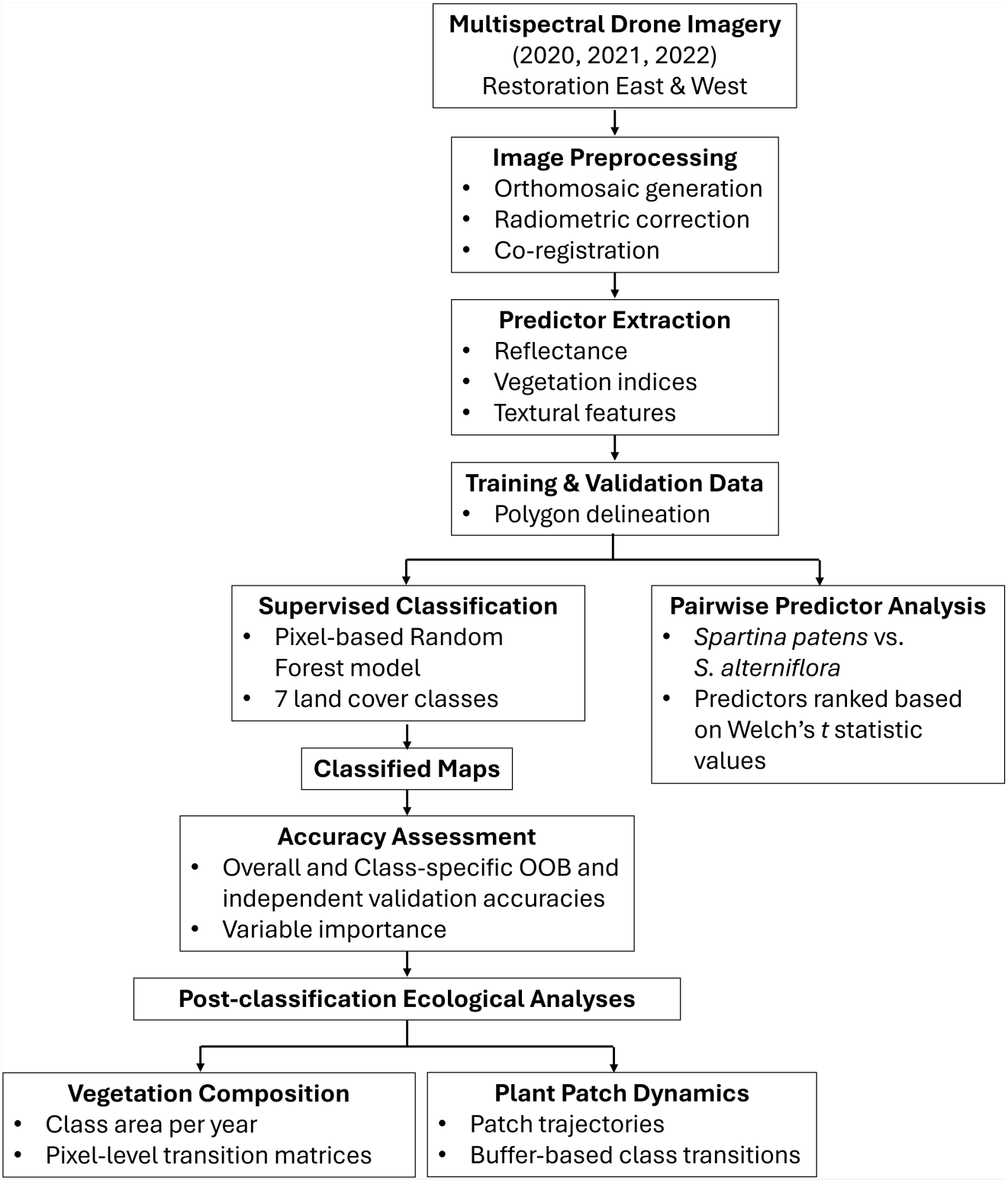

Figure 2

Methodological workflow used to generate annual land-cover maps and conduct ecological and predictor-based analyses at Restoration East and Restoration West, Aulac, from 2020 to 2022. Training and validation data consisted of manually delineated polygons representing relatively homogeneous land-cover patches identified using field observations and UAV imagery. Polygon size varied with patch size and spatial heterogeneity. Polygon samples were used to train and independently validate the

Random Forest classifications and to extract image-derived predictor values for comparisons of *S. patens* with dense and sparse *S. alterniflora*.

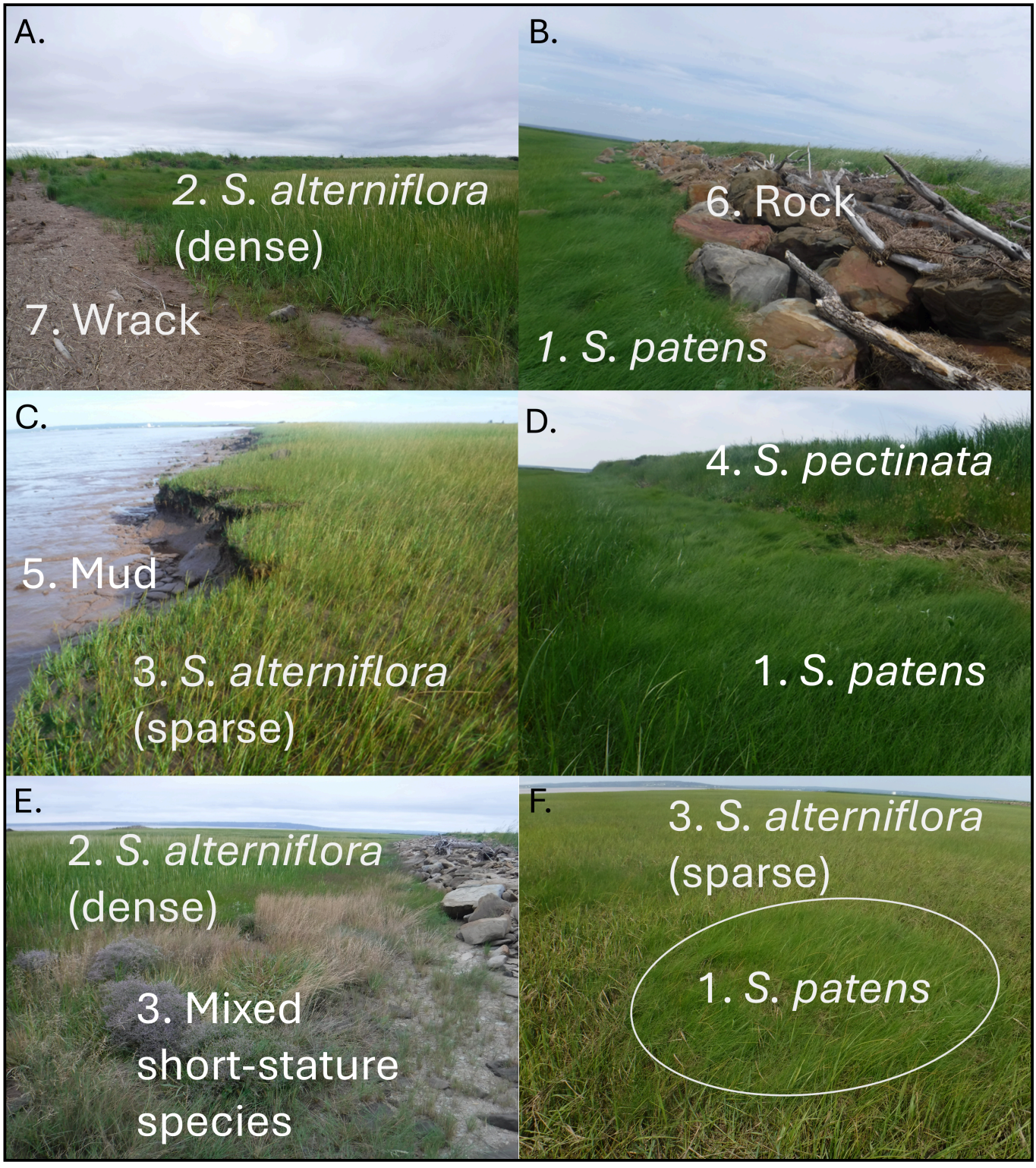

Figure 3

Field photographs of representative vegetation and surface-cover classes used in the seven-class land-cover classifications at the Aulac salt marsh restoration sites. Panels show characteristic species

composition and structural features associated with each class: (A) dense *Spartina alterniflora* adjacent to wrack accumulation; (B) *S. patens* occurring near rock and woody debris along the dike margin; (C) sparse *S. alterniflora* along a mudflat margin; (D) *S. patens* adjacent to *S. pectinata* at the elevated dike edge; (E) mixed low-stature vegetation among dense and sparse *S. alterniflora*; and (F) an *S. patens* patch embedded within sparse *S. alterniflora*.

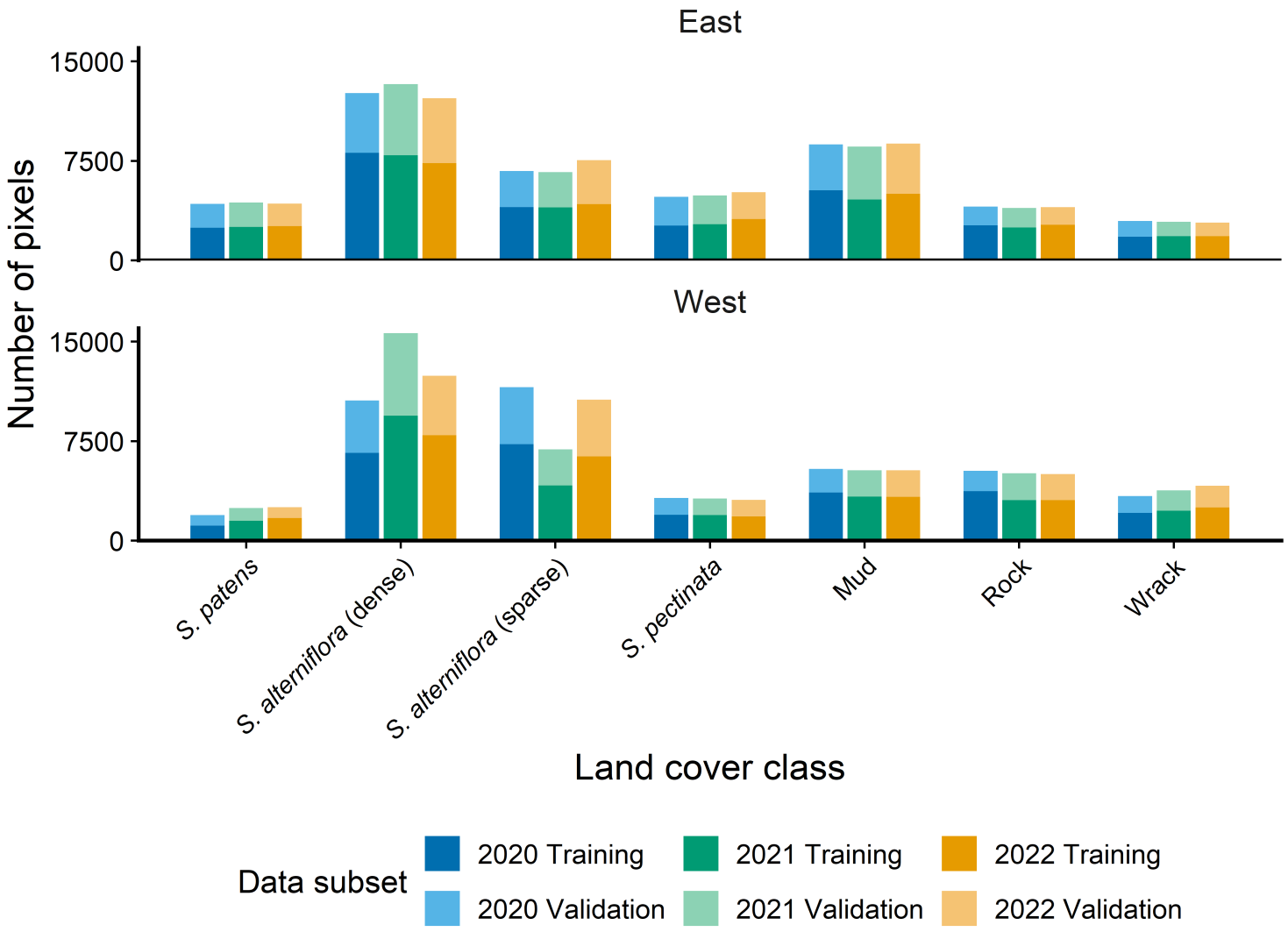

Figure 4

Number of pixels used to train and independently validate the annual seven-class Random Forest classifications at Restoration East and Restoration West, Aulac, from 2020 to 2022. Bars show the distribution of training and validation pixels among land-cover classes for each site and year. Axis labels are abbreviated: *S. alterniflora* (sparse) represents the sparse *S. alterniflora*–mixed low-stature vegetation class, and *S. pectinata* represents the *S. pectinata*–elevated dike edge vegetation class (Table 1).



Figure 5

Classified land cover maps for Restoration East in Aulac, for 2020, 2021, and 2022 using 7-classes (Table 1). Maps were generated using supervised Random Forest classifications of multitemporal predictors derived from June, July, and August multispectral UAV imagery (Tables S1 & S2).

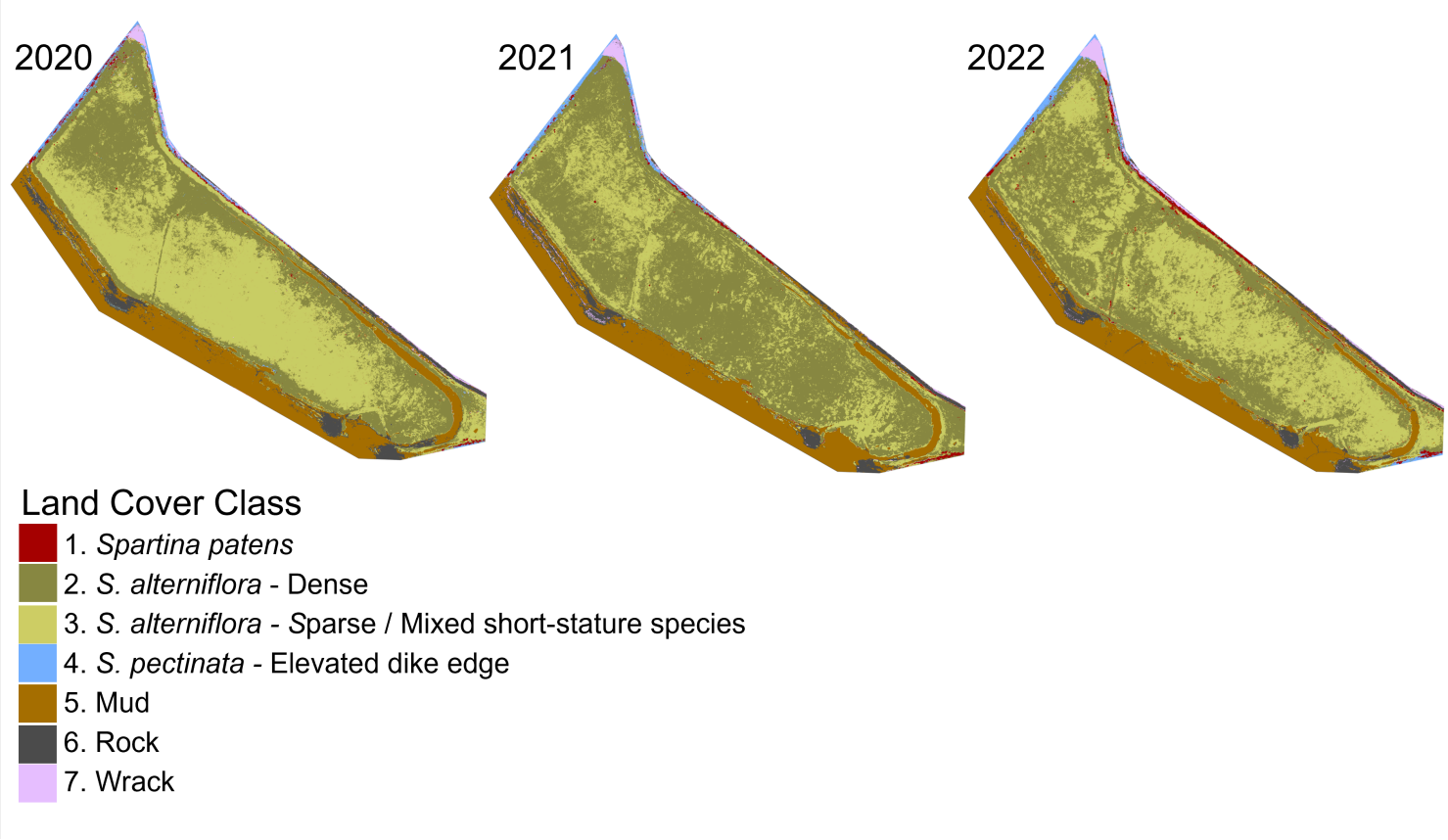

Figure 6

Classified land cover maps for Restoration West in Aulac, for 2020, 2021, and 2022 using 7-classes (Table 1). Maps were generated using supervised Random Forest classifications of multitemporal predictors derived from June, July, and August multispectral UAV imagery (Tables S1 & S2).

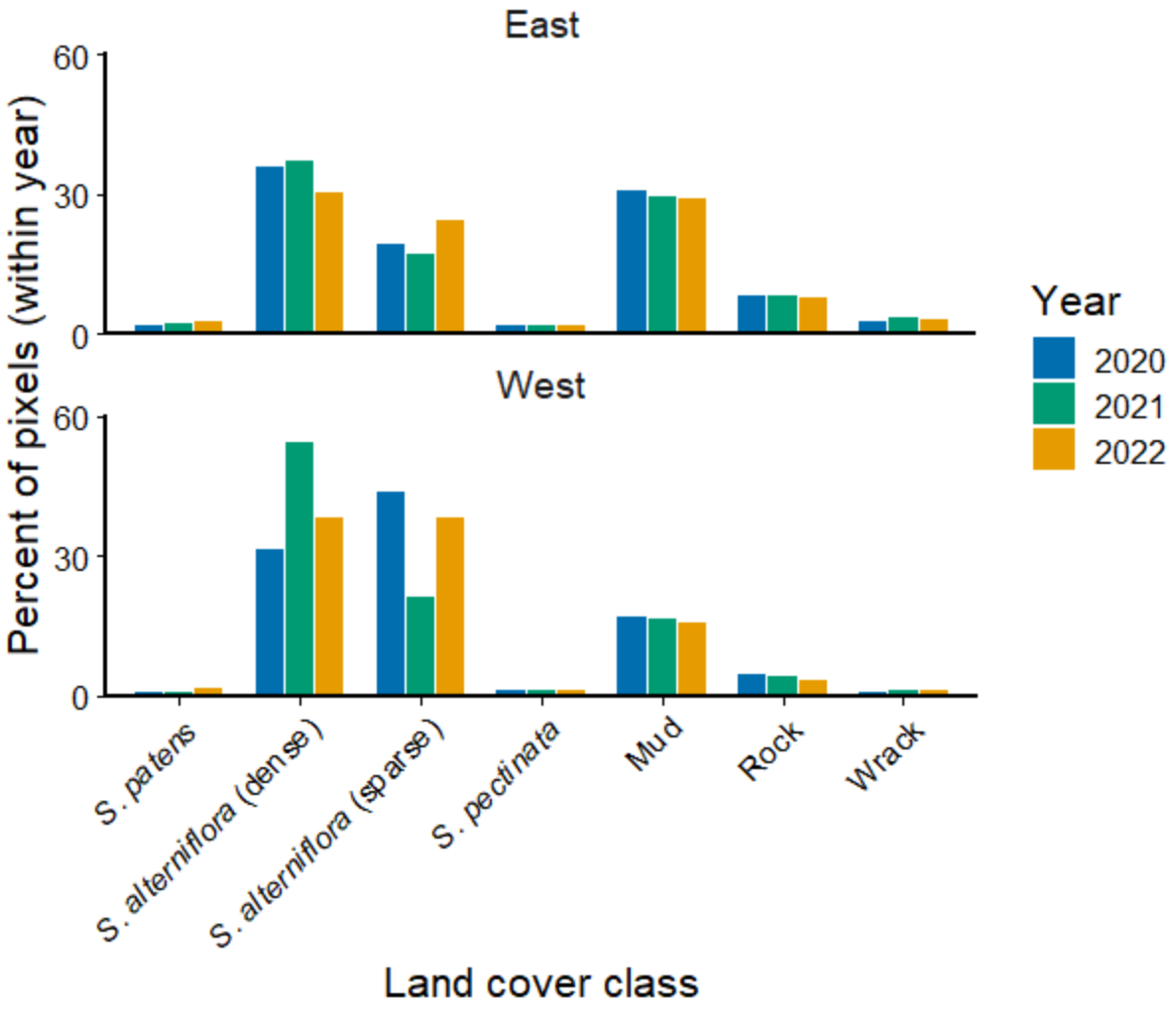

Figure 7

Percentage of classified pixels assigned to each land-cover class at the Restoration East and Restoration West salt marsh restoration sites, Aulac, from 2020 to 2022. Percentages represent the distribution of classified pixels within each site-year. The classifications contained approximately 18.3 million pixels at Restoration East and 29.6 million pixels at Restoration West. Axis labels are abbreviated: *S. alterniflora* (sparse) represents the sparse *S. alterniflora*–mixed low-stature vegetation class, and *S. pectinata*represents the *S. pectinata*–elevated dike edge vegetation class (Table 1). See also Table S15.

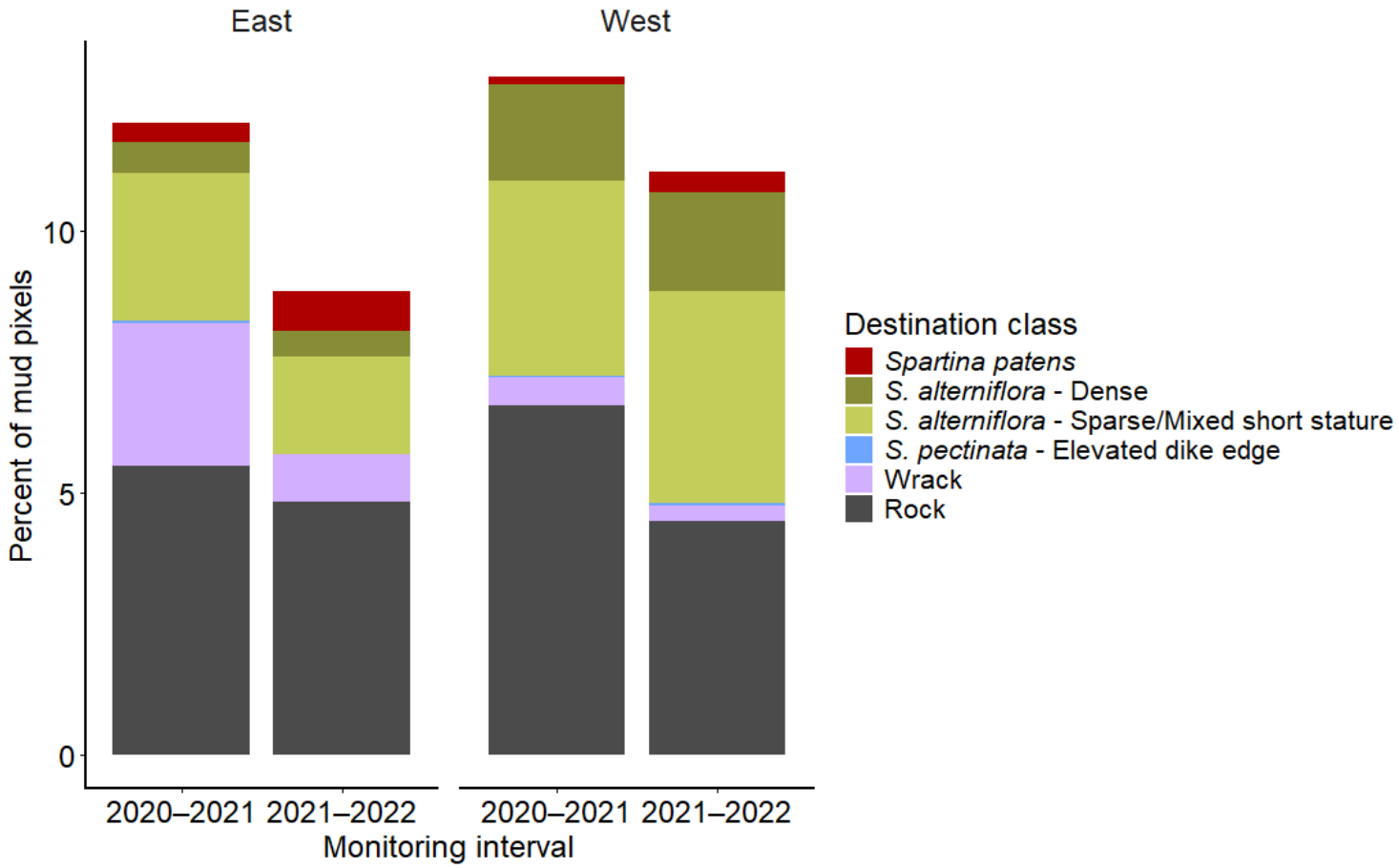

Figure 8

Percentage of pixels classified as mud at the beginning of each monitoring interval (2020–2021 and 2021–2022) that were classified as another land-cover class at the end of the interval at Restoration East and Restoration West, Aulac. Percentages were calculated relative to the total number of mud pixels at the beginning of each interval. Mud pixels that remained mud (87.1–91.2%) are excluded; consequently, the bars do not sum to 100%. All mud pixels within the classified image extents were included. See Tables S16–S22.

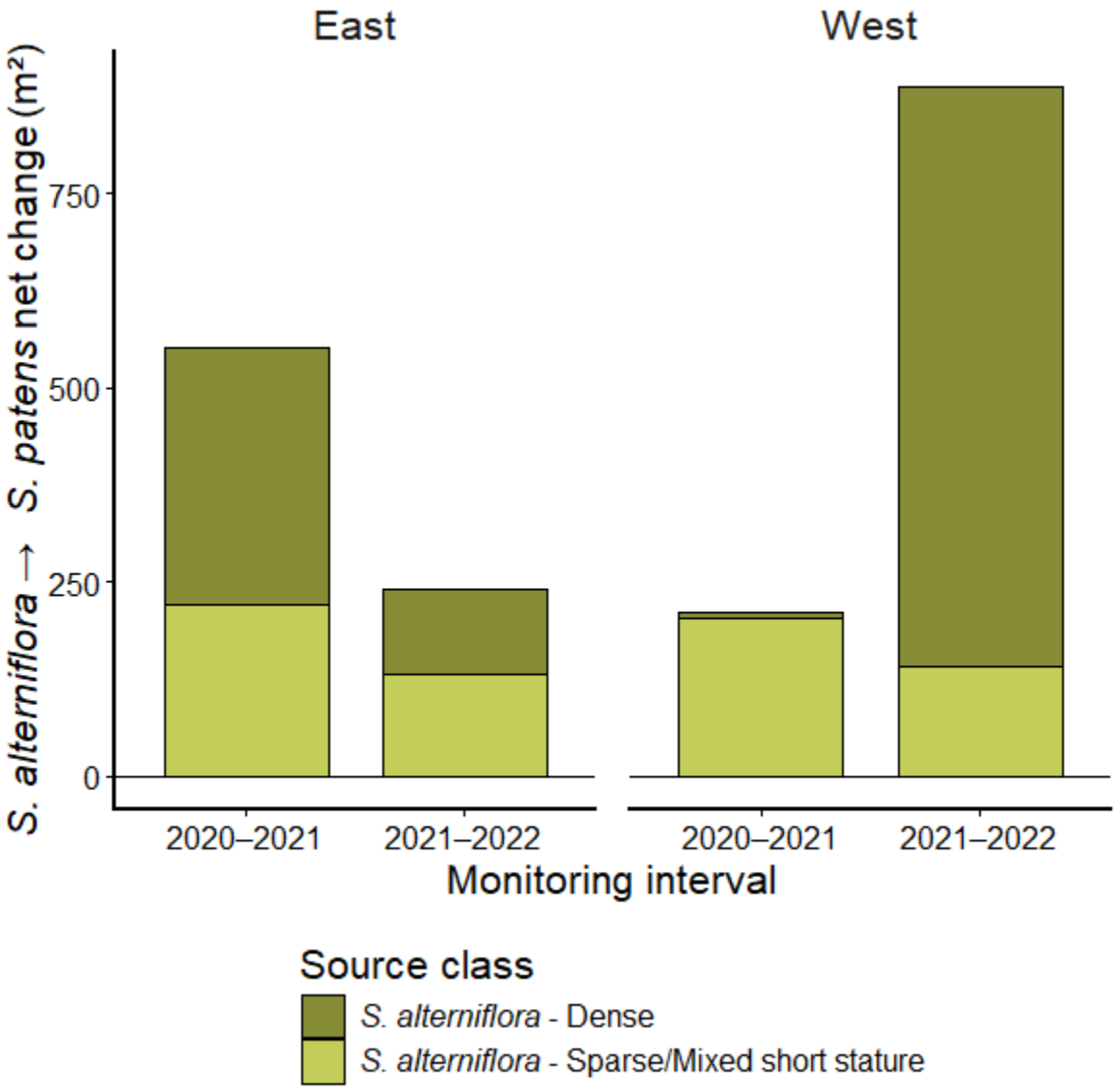

Figure 9

Net change in area (m²) of transitions from *Spartina alterniflora* to *Spartina patens* across monitoring intervals (2020–2021 and 2021–2022) at the salt marsh restoration sites East and West, in Aulac. See also Tables S17–S22. Bars represent contributions from dense and sparse/mixed short-stature *S. alterniflora* source classes. Positive values indicate that transitions to *S. patens* exceeded transitions in the reverse direction; negative values indicate that transitions in the reverse direction exceeded transitions to *S. patens*. Transition areas were derived from pixel counts assuming a ground sampling distance of 7.4 cm (1 pixel = 0.005476 m²).

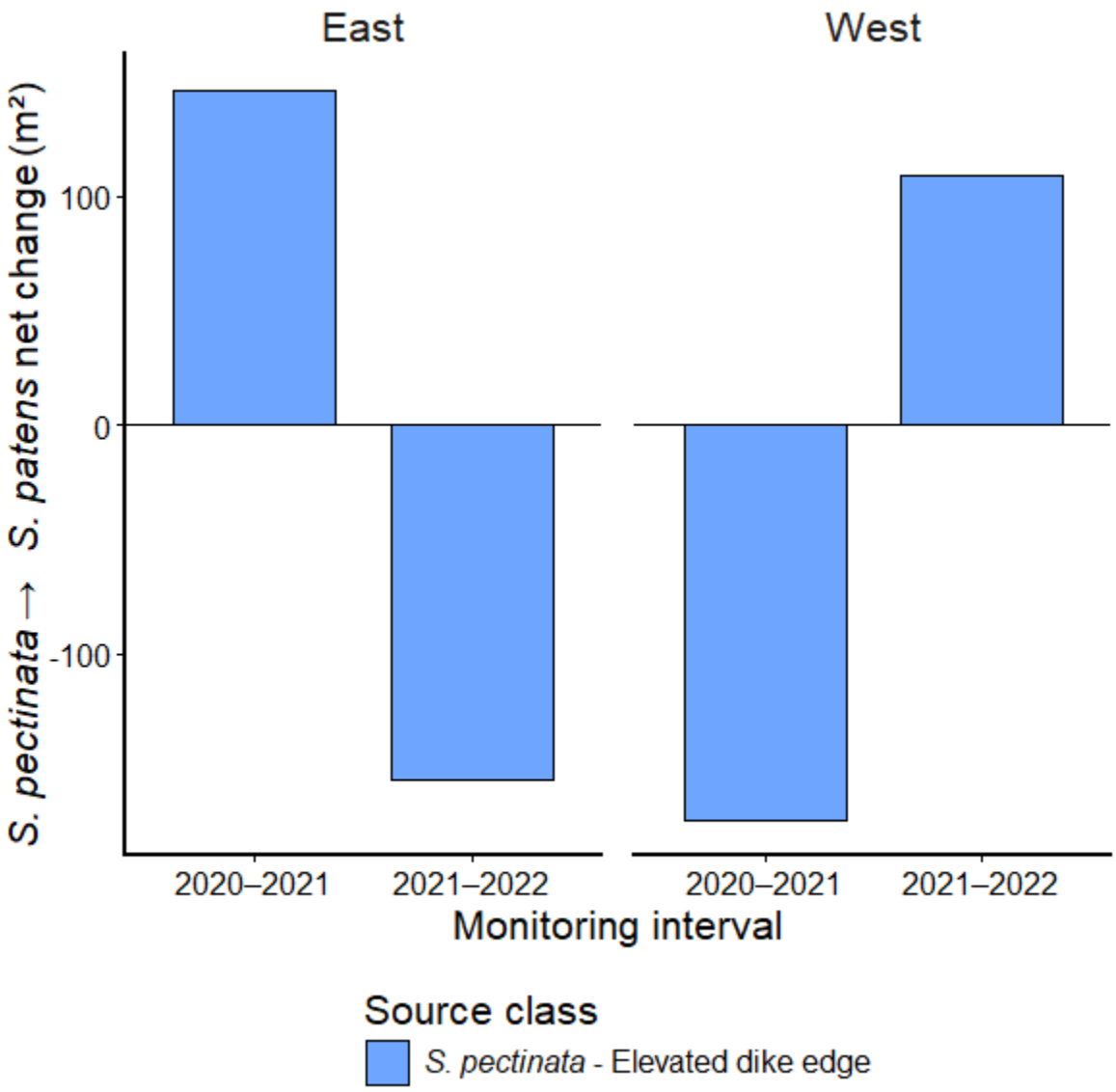

Figure 10

Net change in area (m²) of transitions from *Spartina pectinata* (and elevated dike edge vegetation) to *Spartina patens* across monitoring intervals (2020–2021 and 2021–2022) at for the salt marsh restoration sites East and West, in Aulac. See also Tables S17–S22. Positive values indicate that transitions to *S. patens* exceeded transitions in the reverse direction; negative values indicate that transitions in the reverse direction exceeded transitions to *S. patens*. Transition areas were derived from pixel counts assuming a ground sampling distance of 7.4 cm (1 pixel = 0.005476 m²).

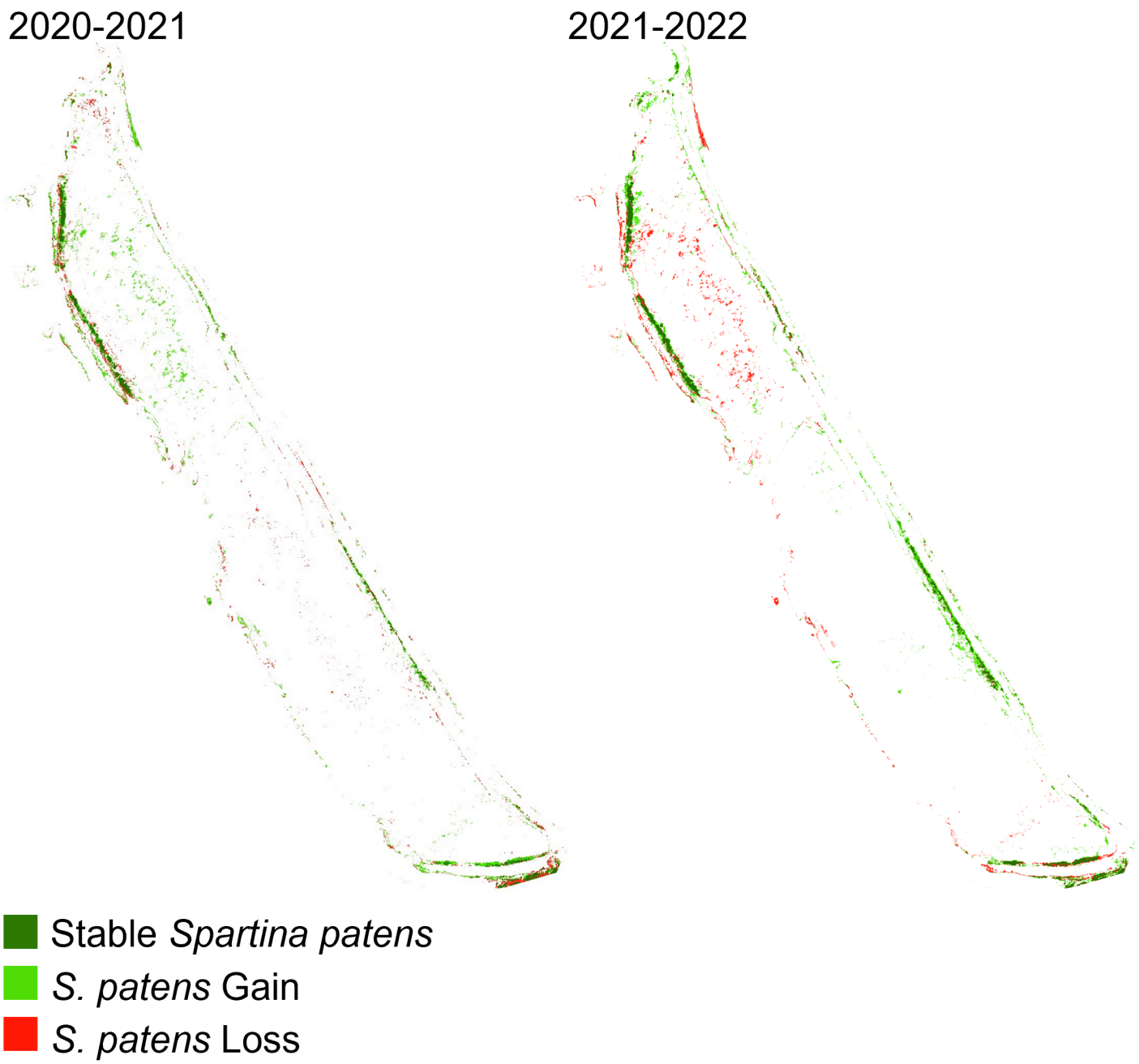

Figure 11

Spatial distribution of persistent *Spartina patens*, gains, and losses at Restoration East, Aulac, during the 2020–2021 and 2021–2022 monitoring intervals. Stable pixels were classified as *S. patens* in both years of an interval, gains were classified as *S. patens* only in the later year, and losses were classified as *S. patens* only in the earlier year.

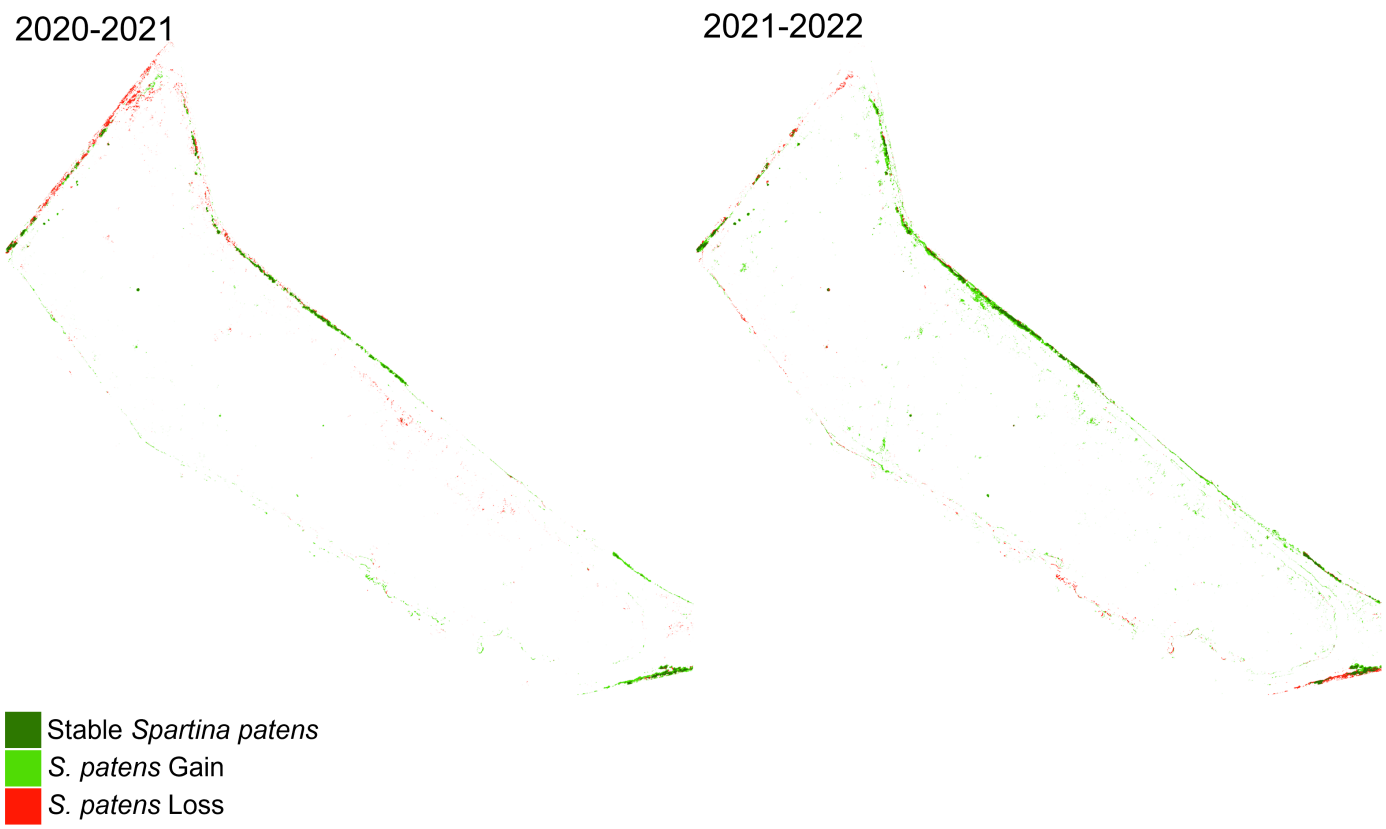

Figure 12

Spatial distribution of persistent *Spartina patens*, gains, and losses at Restoration West, Aulac, during the 2020–2021 and 2021–2022 monitoring intervals. Stable pixels were classified as *S. patens* in both years of an interval, gains were classified as *S. patens* only in the later year, and losses were classified as *S. patens* only in the earlier year.

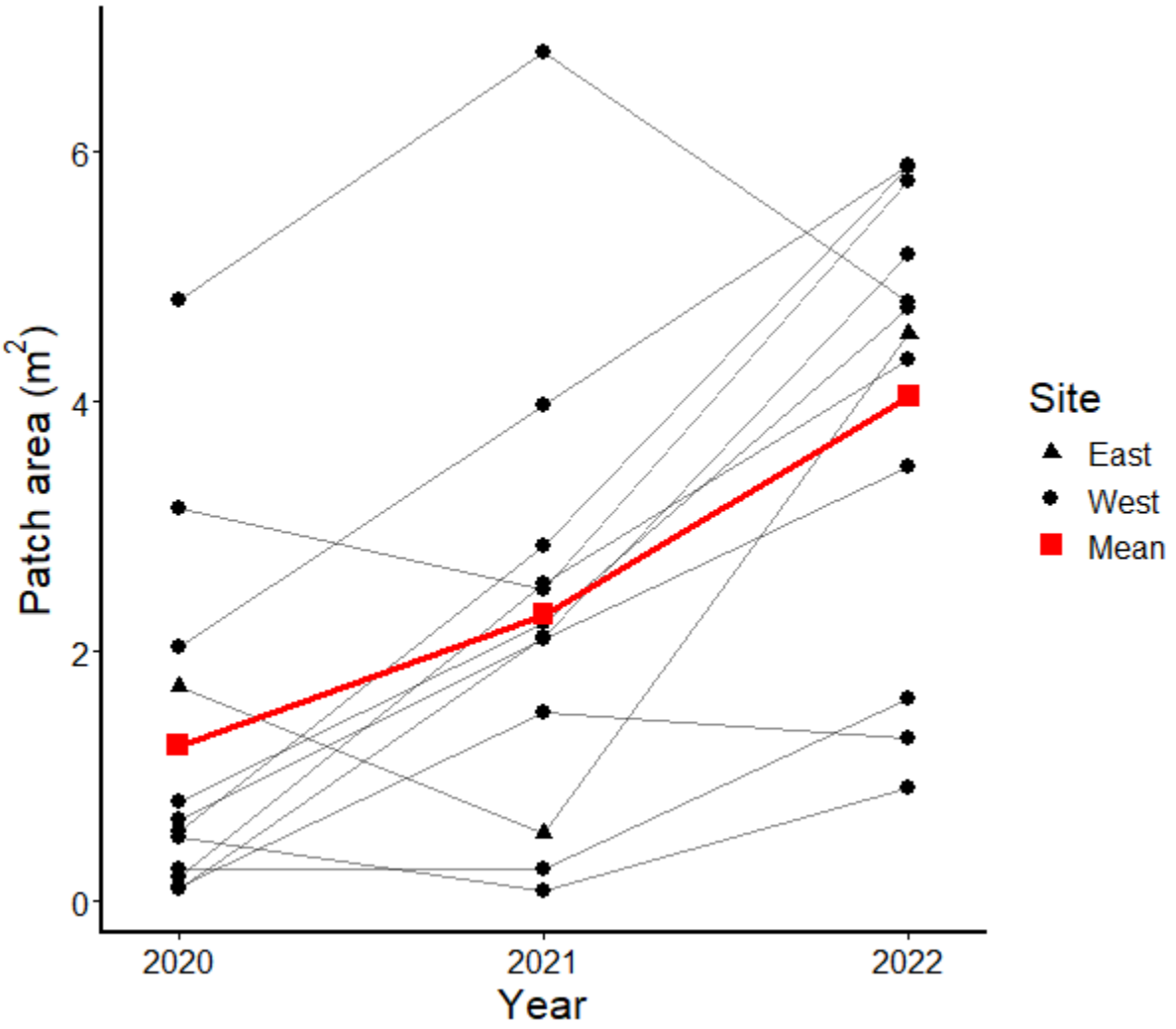

Figure 13

Area (m²) of 12 field-identified *Spartina patens* patches occurring within the salt marsh restoration sites East and West in Aulac, from 2020–2022, derived from classified multispectral imagery (Norris et al. 2022b, Stack Mills et al. 2023). Black lines represent individual patch trajectories (triangles = East; circles = West). The red line and squares indicate the overall mean patch area across both sites for each year (*n* = 12 patches; 11 in Restoration West and 1 in Restoration East).

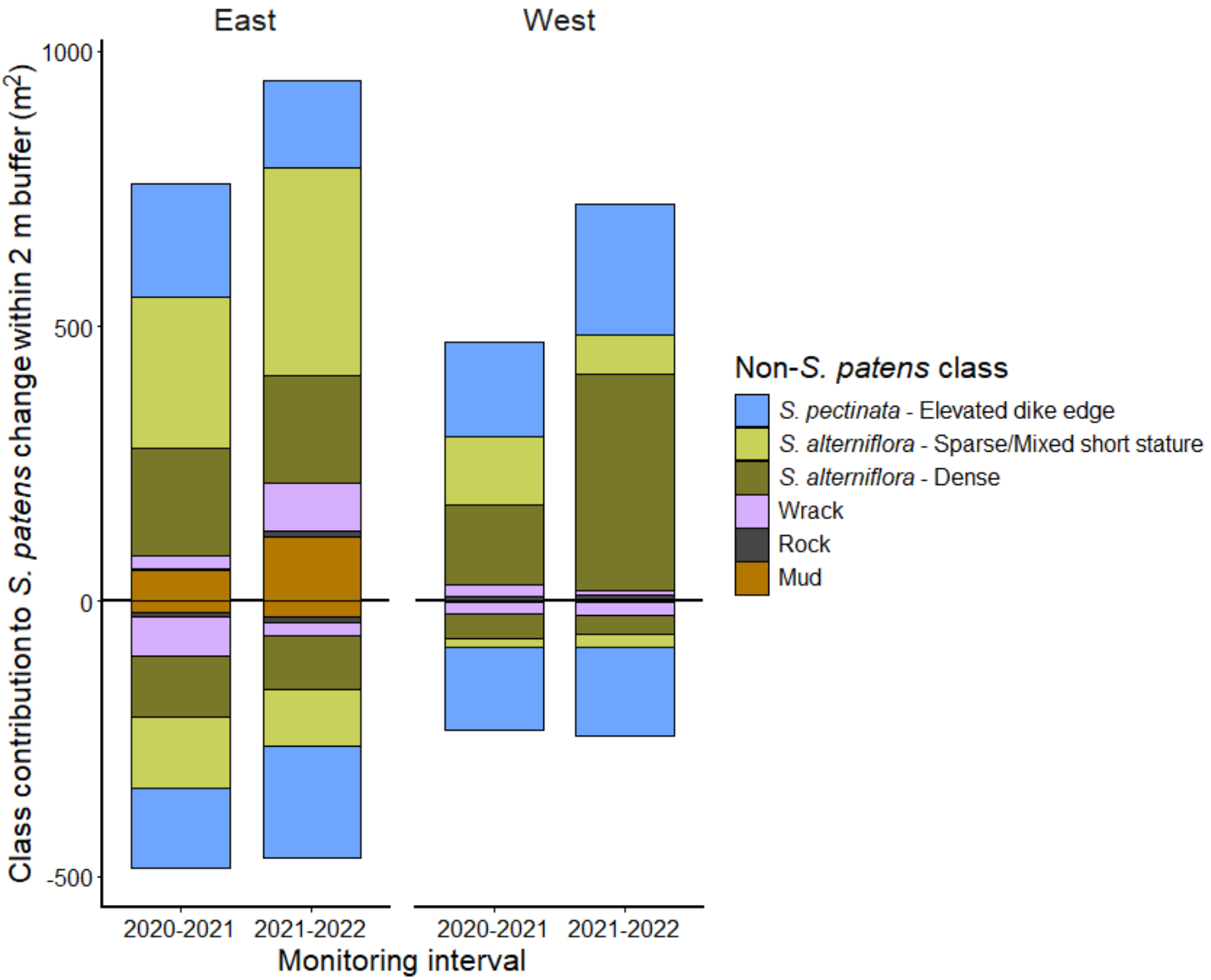

Figure 14

Class-level contributions to changes in *Spartina patens* area (m²) within a 2-m buffer surrounding stable *S. patens* patch cores occurring within the salt marsh restoration sites East and West in Aulac, NB, across monitoring intervals (2020–2021 and 2021–2022). Stable patches were defined as continuous areas of *S. patens* cover persisting between years and exceeding 0.249 m² in area (range: 0.25–127 m²; related to dark green pixels in Figures 11–12). The analysis included 269 and 274 stable patches in Restoration East, and 113 and 134 stable patches in Restoration West for the 2020–2021 and 2021–2022 intervals, respectively. Bars show the area of non-*S. patens* classes associated with gains (positive values) and losses (negative values) of *S. patens* adjacent to the stable *S. patens* patches. Areas were derived from pixel counts using a spatial resolution of 7.4 cm per pixel (0.005476 m² per pixel).

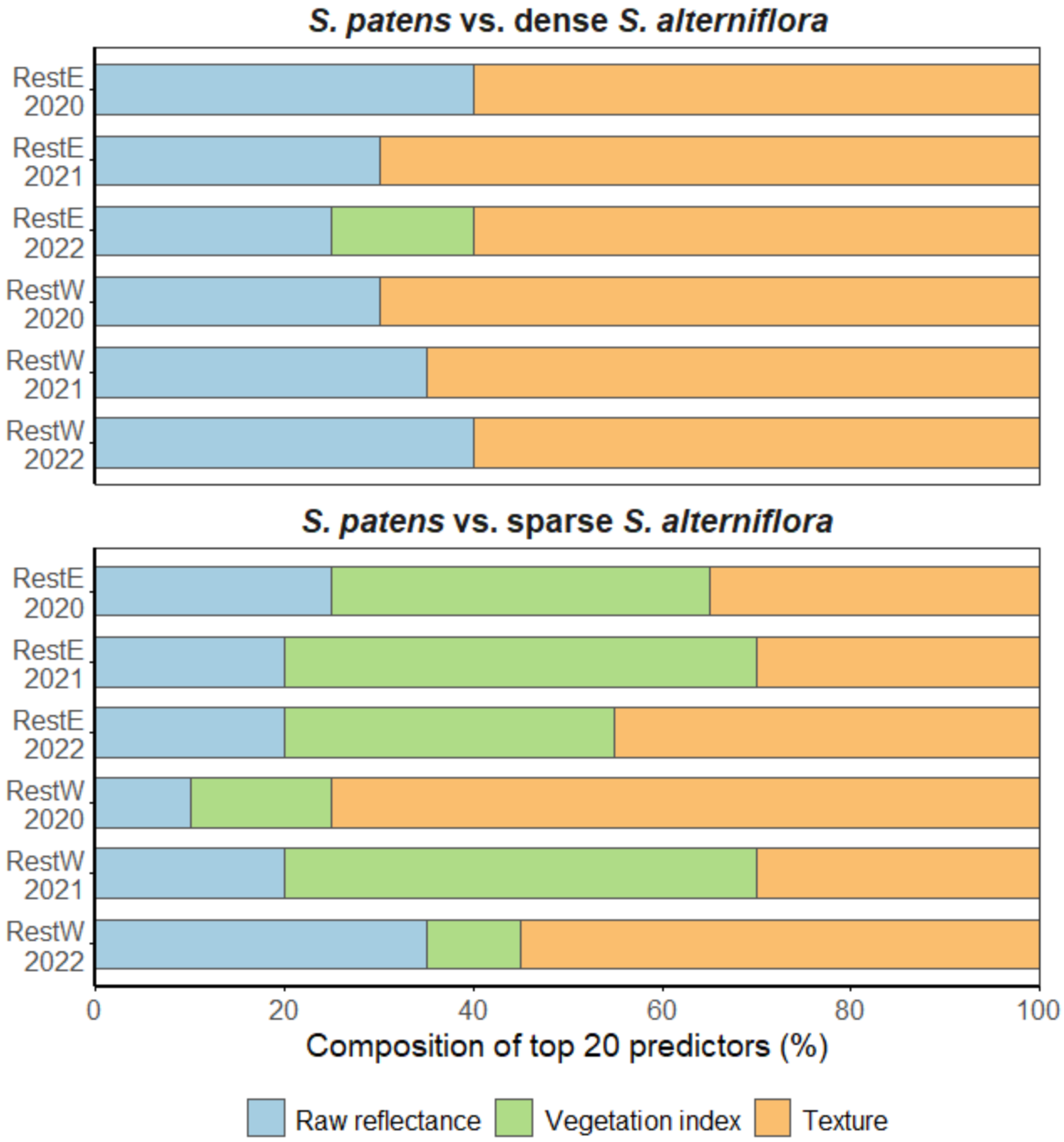

Figure 15

Composition of the 20 highest-ranked predictor variables distinguishing *Spartina patens*from dense and sparse *S. alterniflora* within each site-year combination (Restoration East and Restoration West, 2020–2022) at Aulac; see Table S23 and Figures S4–S15. Predictor variables are grouped into three categories: raw reflectance bands, vegetation indices, and textural features. Percentages represent the proportion of the 20 highest-ranked predictors belonging to each category within each site-year comparison.

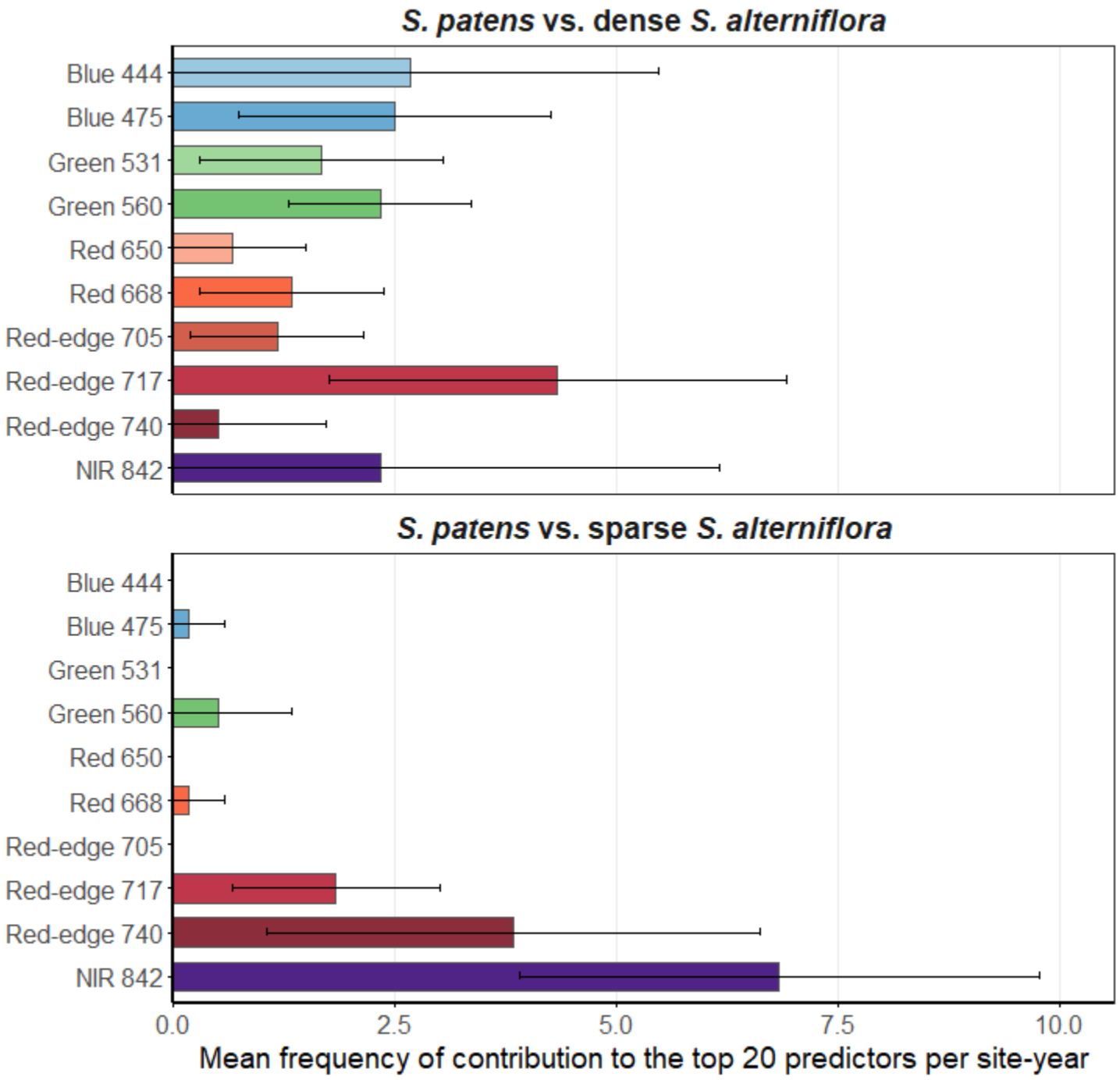

Figure 16

Contributions of original spectral bands to the highest-ranked predictor variables distinguishing *Spartina patens* from dense and sparse *S. alterniflora*across six site-year combinations (Restoration East and Restoration West, 2020–2022) at Aulac. Bars show the mean frequency with which each original spectral band contributed to the top 20 predictors per site-year (n = 6); error bars represent ±1 SD. Contributions include both raw reflectance bands and bands used to derive vegetation indices and textural features. Predictor-type composition is summarized in Figure 15 and Table S23, and site-year-specific predictor rankings are presented in Figures S4–S15.

Supplementary Files

This is a list of supplementary files associated with this preprint. Click to download.

- SupplementaryV34Aug2026.pdf